Optical Engineering

OpticalEngineering.SPIEDigitalLibrary.org

Laser radar: historical prospective—from the East to the West

Vasyl Molebny
Paul McManamon
Ove Steinvall
Takao Kobayashi
Weibiao Chen

SPIE.

Vasyl Molebny, Paul McManamon, Ove Steinvall, Takao Kobayashi, Weibiao Chen, "Laser radar: historical prospective—from the East to the West," *Opt. Eng.* **56**(3), 031220 (2016), doi: 10.1117/1.OE.56.3.031220.

Optical Engineering 56(3), 031220 (March 2017)

REVIEW

Laser radar: historical prospective—from the East to the West

Vasyl Molebny,[a] Paul McManamon,[b,*] Ove Steinvall,[c] Takao Kobayashi,[d] and Weibiao Chen[e]
[a]Academy of Technological Sciences of Ukraine, 42 Glushkov Avenue, Kiev 03187, Ukraine
[b]University of Dayton, 4161 Spruce Pine Court, Dayton, Ohio 45424, United States
[c]FOI (Swedish Defence Research Agency), Department of Electro-Optics, Olaus Magnus Väg 42, 581 11 Linköping, Sweden
[d]University of Fukui, Higashiyama 1031-6, Gotenba, Shizuoka 412-0024, Japan
[e]Shanghai Institute of Optics and Fine Mechanics, Chinese Academy of Sciences, P.O. Box 800-211, Qinghe Road, No. 390, Jiading, Shanghai 201800, China

Abstract. This article discusses the history of laser radar development in America, Europe, and Asia. Direct detection laser radar is discussed for range finding, designation, and topographic mapping of Earth and of extra-terrestrial objects. Coherent laser radar is discussed for environmental applications, such as wind sensing and for synthetic aperture laser radar development. Gated imaging is discussed through scattering layers for military, medical, and security applications. Laser microradars have found applications in intravascular studies and in ophthalmology for vision correction. Ghost laser radar has emerged as a new technology in theoretical and simulation applications. Laser radar is now emerging as an important technology for applications such as self-driving cars and unmanned aerial vehicles. It is also used by police to measure speed, and in gaming, such as the Microsoft Kinect. [DOI: 10.1117/1.OE.56.3.031220]

Keywords: laser radar; direct detection laser radar; coherent laser radar; environmental lidar; laser microlaser radar; ghost laser radar.

Paper 161271SSPV received Aug. 11, 2016; accepted for publication Nov. 11, 2016; published online Dec. 28, 2016.

1 Introduction

Laser radar (also called ladar for laser detection and ranging, lidar for light detection and ranging, or opdar for optical detection and ranging) started most of its development in the early 1960s, shortly after the invention of the laser. There had been some earlier lidar development prior to the invention of the laser, but the laser has been a real enabler. Laser radar has become relatively inexpensive and reliable, and has very rich phenomenology, making laser radar competitive compared to alternative sensor technologies, such as passive electro-optical sensors or microwave radar. Laser radar started operating in the visible region (ruby laser) and then appeared in the near infrared (Nd:YAGlasers) to the thermal infrared (CO_2 laser). Many laser radars are now being developed in the eye safe short-wave infrared region ($\sim$1.5 μm).

Numerous publications accompanied the maturing of laser radar, bringing to life new journals, new professional meetings, symposia and conferences, such as "Laser Radar Technologies and Applications" managed by the SPIE as part of the Defense and Commercial Sensing symposium, which includes special laser radar courses for participants.[1] Laser radar became the topic for new fundamental books[2–5] and reports,[6] as well as a subject taught at the universities.[7] New technologies appeared based on laser radar principles, such as optical coherence tomography (OCT) and digital holography. The range of most laser radar applications is from micrometers[8] to tens of kilometers.

Overviews on the history of laser radar development appeared concerning Europe,[9] the United States,[10] the former Soviet Union (FSU),[11,12] Japan,[13] and China.[14] This paper combines and updates those histories. We have limited our examples to a sample of laser radar techniques and applications instead of trying to cover the whole field. It is still a daunting organizational task to cover the world history of laser radar technology for more than 50 years.

*Address all correspondence to: Paul McManamon, E-mail: paul@excitingtechnology.com

2 Direct Detection Laser Radars and Designators

2.1 *First Steps of Range Finders*

A laser range finder is the simplest kind of laser radar. It uses a single detector to determine the range to a target based on the round-trip time-of-flight of a laser pulse to and from the object. Because we know the speed of light, we can calculate range. The idea to use short pulses of light to measure distance was brought out by Lebedev.[15] Short pulses allow excellent range resolution. The prototype used a specially developed interference modulator to obtain short pulses of light in 1936. A range up to 3.5 km was measured with the accuracy of 2 to 3 m. In 1963 to 1964, laser-based rangefinders were developed using ruby and gallium arsenide in the same lab used by Lebedev in the 1930s, the Vavilov Optics State Institute (GOI) in Leningrad (now St. Petersburg).

Range finders, proximity fuzes, and weapon guidance were the first military laser systems in the late 1960s and early 1970s. The early ruby lasers were high cost, with poor efficiency, and with eye safety issues. Later short pulse, high-energy, and highly collimated monochromatic beams became available as Q-switched lasers revolutionized laser radar capabilities.

In Sweden, laser research with a ruby laser started at Swedish Defense Research Establishment (FOI) in 1961. In the industry, the pioneers were ASEA and LM Ericsson. In

1968, Ericsson delivered laser range finders to the Swedish Coastal Artillery for operational use. Bofors developed laser range finders for the infantry canon vehicle IKV 91 and for the BOFI system in co-operation with Hughes Aircraft. Later, ASEA developed cloud altimeters for the civilian and military markets. During the early 1970s, Bofors developed a successful antiaircraft missile beam rider system, the RBS 70, which later was modified into the RBS 90 and sold worldwide. The world's first laser beam rider surface to air missile, SAM, to enter service was developed at Bofors and contained laser sensing. During the late 1970s, Ericsson developed laser-based proximity fuses for the Sidewinder missile. Ericsson also developed a laser tracking system, but that laser application was soon overtaken by video trackers.

In Norway, the Norwegian Defense Research Establishment transferred their knowledge to Simrad Optronics, which became famous for their laser range finder built-in to a handheld binocular. More recently, the company developed a family of range finders for target location and fire control.

In the United Kingdom, Royal Signals and Radar Establishment (RSRE) pioneered military laser development. An excellent review on the early laser range finder development was published by Forrester and Hulme.[16] They claim that the LF-2 ruby tank laser sight was the first laser system in the world to be in large quantity production. It was developed primarily for use with the Chieftain main battle tank for the British army, but was widely used on other tanks, such as Vickers MBT, Centurion, Scorpion, and Chieftain derivatives. The original equipment used was a ruby laser with a spinning prism Q-switch, although a later version used a passive Q-switched YAG (LF-11).

In 1968, Ferranti (now Leonardo Finmeccanica) developed the world's first fully stabilized laser system incorporating a Nd:YAG laser range finder and marking target seeker. The marking target seeker is a unit on the aircraft which locks onto a laser designated target. This equipment was a part of the weapon aiming systems of Jaguar, Harrier, and Tornado aircraft. The 1.06-μm laser transmitter power was generated by an electro-optically Q-switched Nd:YAG laser capable of operating at 10- or 20-Hz repetition rate.

One of the first Soviet laser range finders, BD-1 (Fig. 1), was described in a later SPIE publication.[17] Another example is the KTD 2-2. The technology of laser range finders and laser designators is represented by numerous operational instruments described in a later publication.[18] They are installed on SU and MIG airplanes as well as helicopters (see Fig. 2). In France, Thales Research and Technology delivered a Nd:YAG laser range finder to the French Official Services in 1967. The laser range finder was installed on the AMX 13 tank for field tests.[19] In the 1970s, Thomson and Cilas developed an airborne target illumination system that demonstrated the ability to be used on a single seat airplane fighter, and it was later developed into the ATLIS targeting pod.

Germany also developed laser range finders and target designators based on a Nd:YAG laser by Carl Zeiss and Eltro. Military laser research was performed by FGAN-FfO. Many of their early publications were dedicated to laser propagation in the atmosphere.[20]

2.2 *Long Distance Range Finders*

The first laser ranging to the moon was done by MIT Lincoln Laboratory (MIT/LL) in 1962 using a 50 J/pulse Ruby laser. Precise laser ranging to the moon was then done in 1969 from NASA Goddard Space Flight Center in Greenbelt,

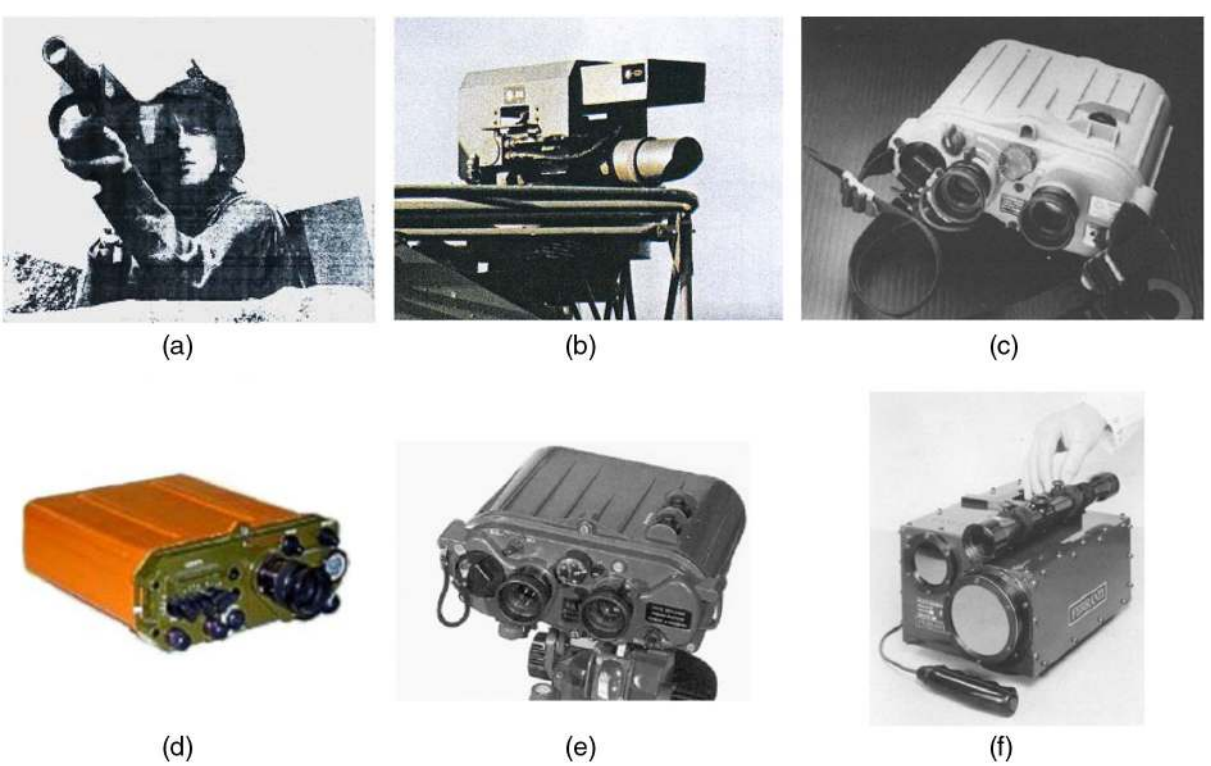

Fig. 1 Examples of early laser range finder (LRF) development. (a) Test equipment for the first Ericsson LRF (1965), (b) LRF for the Swedish Coastal Artillery (1968), (c) Simrad handheld LP-7, (d) LRF KTD 2-2 (Polyus, USSR), (e) LRF BD-1 (Institute # 801, USSR), and (f) Ferranti CO_2 TEA LRF.

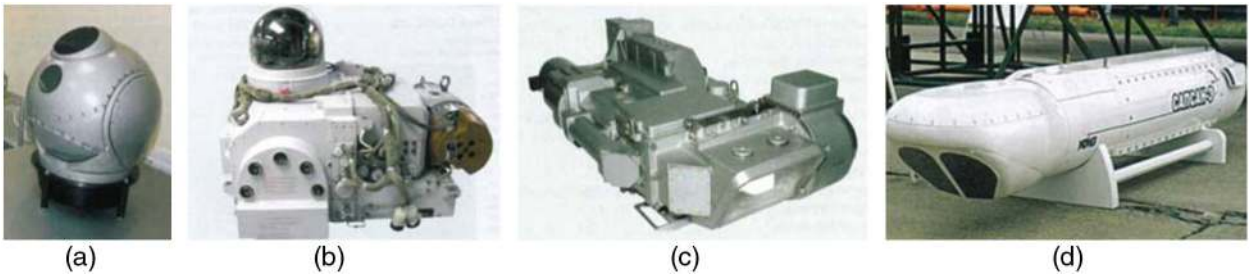

Fig. 2 Examples of the Soviet/Russian range finder/designator laser radars: (a) Samsheet-50 range finder/designator for Ka-52 helicopter, (b) 31E-MK electro-optic system for Su-30 fighter, (c) Shkval series for Su-25T, Su-25TM/Su-39, and Ka-50, and (d) pod mounted Sapsan-E for air-to-surface MiG and Su missions.

Maryland. It used a retroreflector positioned on the Moon by the Apollo 11 astronauts. By beaming laser pulses at the reflector from Earth, scientists have been able to determine the distance to that spot on the moon to an accuracy of about 3 cm. Additional retroreflector packages were landed on the lunar surface by NASA during the Apollo 14 and Apollo 15 missions. French-built retroreflector packages were soft-landed on the lunar surface by Soviet landers.[21]

A retroreflector package was also used in the Japanese Retroreflector in Space (RIS) project, installed on the ADEOS satellite (National Space Development Agency of Japan, present: Japan Aerospace Exploration Agency) and launched in August 1996. The retroreflector had a curved mirror surface to compensate for the velocity aberration due to the satellite movement. A ground-based transmitter–receiver system used a transversally excited atmospheric pressure (TEA) CO_2 laser and a HgCdTe detector having a 1.5-m diameter high-precision tracking telescope at the Communication Research Laboratory (now called the National Institute of Information and Communications Technology) in Kokubunji, Tokyo. The absorption spectra of atmospheric ozone were successfully measured in the 10-μm wavelength region using the reflection from the RIS.[22]

In the FSU, long-distance measurements with lasers started in 1962 by the Vympel Design Bureau, in co-operation with Lebedev Physics Institute. Its first experiments in 1967 allowed laser ranging of a Tu-134 airplane, equipped with optical retroreflectors.[9] Ten years later, a giant laser radar LE-1 was tested at Sary-Shagan, and its main goal was antimissile defense. It tracked the satellite Molniya and measured the distance to it without any retroreflector.

The FSU LE-1 had a multichannel transmitter (49×4) and a multichannel receiver with an array of 196 range-gated photomultipliers, each having its own optical system. The switch is made of a block of four optical wedges rotating at 80 Hz. The LE-1 multibeam was controlled by means of a fast 2-D scanner consisting of two mirrors driven by stepping motors. The mirrors kept the beam stable during the transmit–receiver cycles. Each laser consisted of a master oscillator/power amplifier with identical ruby crystals and a KDP electro-optical switch. Output pulse energy was 1 J, pulse repetition frequency (PRF) of each laser was 10 Hz, and pulse duration was 30 ns. The optical train was designed by Geofizika Central Design Bureau in cooperation with Vavilov Optical Institute. The Cassegrain telescope with 1.2 m of main mirror aperture and 21 arc min field-of-view provides target tracking in the upper hemisphere. It was designed and manufactured by LOMO. The telescope drives the operation with an angular velocity up to 5 deg/s and angular acceleration up to 1.5 deg/s^2 with a 5′ dynamic error. Velocity aberration is compensated by the tilt of a mirror. The LE-1 laser radar could detect a 1-m^2 target at 400 km.

2.3 *Laser Altimeters*

Time-of-flight measurement is a keystone of laser radar altimeters. The lunar orbiter laser altimeter (LOLA), built by United States NASA, was designed to characterize landing sites and to provide a precise global geodetic grid on the Moon.[23] LOLA's primary measurement is surface topography. The instrument provides ancillary measurements of surface slope, roughness, and reflectance. LOLA is a multibeam laser altimeter that operates at a wavelength of 1064.4 nm with a 28-Hz pulse repetition rate. A single laser beam is split by a diffractive optical element into five output beams [Fig. 3(a)], each of which has a 100-mrad divergence and illuminates a 5-m diameter spot from the mapping orbit, resulting in a total sampling rate of the lunar surface of 140 measurement/s. Backscattered pulses are detected by the receiver, which images the five-spot pattern onto separate optical fibers, each of which relays the received signal to a distinct silicon avalanche photodiode (APD) detector. An example of lunar profiles is shown in Fig. 3(b).

The laser spots form a cross pattern on the lunar surface, with each beam separated by an angle of 500 mrad and rotated 26 deg about the nadir axis with respect to the spacecraft forward velocity vector. The sample pattern permits calculation of surface slopes along a range of azimuths. A topographic map of the Moon is shown in Fig. 3(c).

To raise the sensitivity of laser radar for automotive applications, Inoue et al.[24] from Toyota used fiber amplifiers both for transmitter and receiver, having designed an instrument with a sensor head 2 cm^2 in size. The transmission optical system consists of a pulsed fiber laser. The peak output power is 10 kW, and the pulse width is 4 ns. The diameter of the scanning mirror is 10 mm. The optical fiber amplifier has a mid-way isolator, and a band-pass filter, to cut down spontaneous emission and to improve the conversion efficiency and noise figure.[25] The resonant frequency of the scanning mirror is 100 Hz and the scanning angle is 40 deg.

The Institute of Space and Astronautic Science (ISAS), Japan, developed various laser altimeters for space and astronautical science use. Figure 4 shows some details of the Hayabusa mission using the Hayabusa lidar launched in 2005.[26,27] Figure 4(a) is a picture of the asteroid Itokawa (size: 540 m $\times$ 270 m $\times$ 210 m) taken by an imager, and

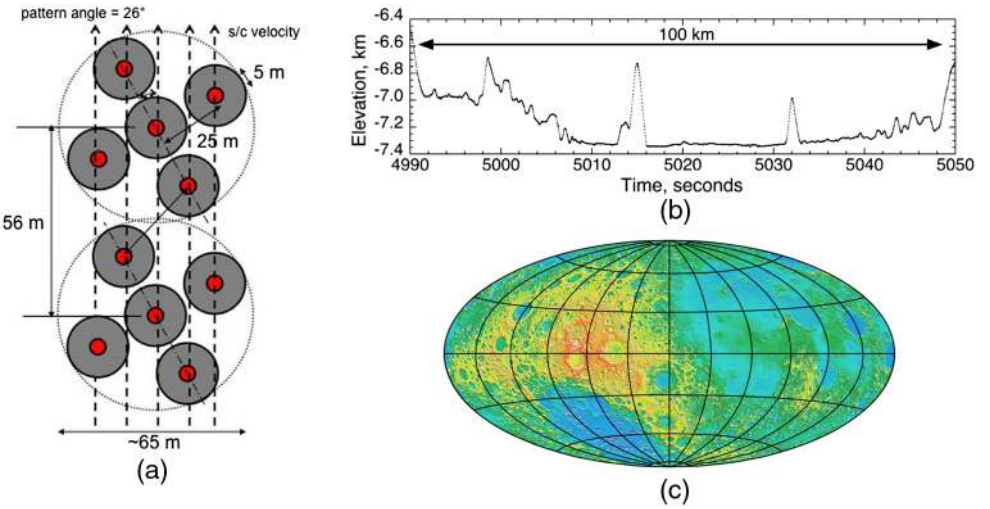

Fig. 3 (a) Lunar orbiter laser altimeter: five output beams, (b) lunar profiles, and (c) topographic map of the Moon.

Fig. 4(b) shows a flight model of ISAS. It operates at 1064 nm with 8 mJ, 1 Hz, 12.5-cm aperture, 3.7 kg, 24 cm × 23 cm × 25 cm). Figure 4(c) shows relative elevation measured by the Hayabusa laser radar. It has a range resolution of ±1 m. The precise elevation measurement of the asteroid was the first in the world. The Hayabusa-2 laser radar was launched in 2015 targeting a near-Earth asteroid named 1999 Ju3.

2.4 *Laser Designators*

The first laser designator is shown in Fig. 5(a). It is a part of the Paveway series of laser guided bombs [Fig. 5(b)]. Since its inception in 1968, the Paveway has revolutionized tactical air-to-ground warfare.[8] These semiactive laser guided munitions, which home in on reflected energy directed from the target, not only drastically reduce the number of munitions required to destroy a target but also feature accuracy, reliability, and cost effectiveness previously unattainable with conventional weapons. NATO forces successfully employed Paveway during the operation Desert Fox and the subsequent patrol of the "no-fly" zones over Iraq, because of its pinpoint accuracy and reduced chances of collateral damage. The Paveway III is the third generation providing the optimum operational flexibility through the use of an adaptive digital auto pilot, large field-of-regard, and highly sensitive seeker. It adapts to conditions of release, flies the appropriate midcourse, and provides trajectory shaping for enhanced warhead effectiveness. When used in conjunction with the BLU-109 or BLU-113 penetrator warheads, Paveway not only optimizes the trajectory and impact angle but also the angle-of-attack.

2.5 *Laser Range Finders and Designators as System Components*

After the initial development of ruby and Nd:YAG laser range finders and target designators, questions about range finder compatibility with FLIR in the 8 to 12 μm region were raised as well as the issue of eye safety. It was desired to measure the range of any target, which can be distinguished by the thermal imager, including, for example, an ability to penetrate mist and smoke. These considerations led to the development of pulsed range finders based on the pulsed CO_2 TEA laser. A CO_2 TEA prototype range finder was developed by RSRE and Ferranti.[28]

The CO_2 TEA range finder was, however, not a success. Only a very few became operational due to a series of problems; among them, the "wet target problem" meaning range loss from wet targets due to low reflectivity at 10.6 μm, the necessity of cooled detectors, expensive optics, and laser life time problems. The main thrust in military laser range finding was soon centered around the wavelength of 1.5 μm utilizing Raman-shifted optical parameter oscillator or

Fig. 4 "Hayabusa" mission using the Hayabusa lidar. (a) A picture of the asteroid "Itokawa" taken by an imager, (b) a flight model, and (c) relative elevation and horizontal distance measured by the Hayabusa lidar.

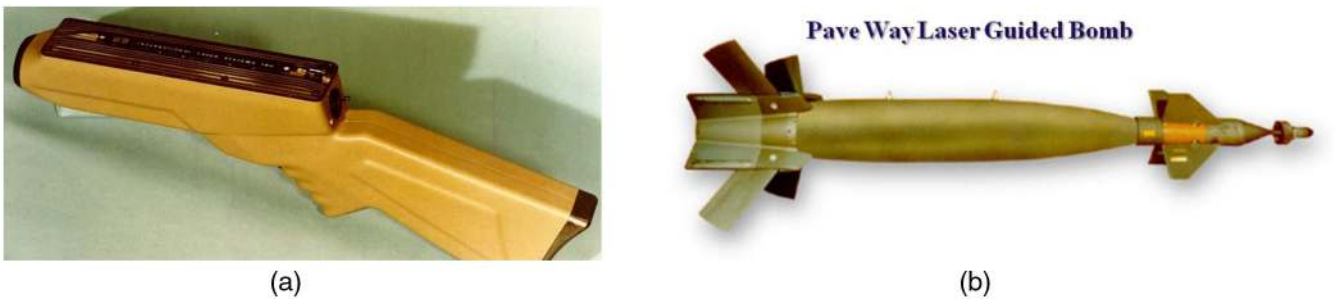

Fig. 5 (a) The first laser target designator (1969) and (b) the first laser guided bomb.

high-pressure gas technology, shifting Nd:YAG from 1.06 to 1.55 μm. Other schemes involved erbium glass or other materials. Starting with an efficient Nd:YAG laser as a pump source, the concept of multifunctional lasers was evolved.[29] The idea was to combine 1.06-μm range finding/designation with laser radar, laser jamming, battlefield identification "friend or foe" and other functions into a compact system centered around one transmitter. In Fig. 6, examples of systems developed in the FSU are shown, incorporating the laser range finders and designators.

2.6 *Noncoherent Wind Measurement*

Low altitude wind profile measurements with a noncoherent laser rangefinder were demonstrated using a simple balloon tracking system, with small (0.25-m diameter) lightweight balloons.[30] Experiments on balloon trajectories demonstrate that laser range detection ($\pm$0.5 m) combined with azimuth and elevation measurements is a simple, accurate, and inexpensive alternative to other wind profiling methods. To increase the maximum detection range to 2200 m, a retroreflector tape was attached to the balloons. Night-time tracking was facilitated by low-power light-emitting diodes (LEDs).

Another example of noncoherent Doppler wind measurement is demonstrated in the paper of Liu et al.[31] Liu is from the Ocean University of Qingdao, China, and some of his collaborators are from NASA Langley Research Center, Hampton, Virginia. A schematic of the lidar transmitter, receiver, and frequency control is shown in Fig. 7. The master oscillator of the system is the two-wavelength diode pumped continuous wave (CW) single-mode tunable Nd:YAGseed laser. The output at 1064 nm is used to seed a Continuum Powerlite 7000 Nd:YAG pulsed laser. The 532-nm output of the seed laser is sent to an iodine filter (cell 1) to control and lock the seed laser frequency. With this setup, the frequency precision is maintained to within 0.2 MHz, corresponding to a wind measurement uncertainty of 5.0 cm/s.

The mobile direct-detection Rayleigh-scatter Doppler lidar (Fig. 8) was developed by the University of Science and Technology of China[32,33] to measure wind fields at a range of 15 to 70 km with a height resolution of 0.2 km below 40 km and 1 km above. This nonscanning system operates at an eye-safe wavelength of 354.7 nm using a frequency tripled 50-Hz Nd:YAG laser. A triple channel is used as a frequency discriminator to determine the wind velocity, two of them being double-edge channels located in the wings of the thermally broadened molecular backscattered signal spectrum, while the third one locks the frequency of the outgoing laser at the cross-point of the double-edge channels.[34] The scanning system can detect the horizontal wind in four directions (north, south, east, west) by scanning the emitting–receiving system.

3 Coherent Laser Radars

3.1 *Airborne Applications*

Coherent laser radars make use of the spatial and temporal coherence properties of laser radiation. By mixing the received signal with an optical local oscillator, the full field can be measured, including both phase and amplitude information, as compared to direct detection, where we only

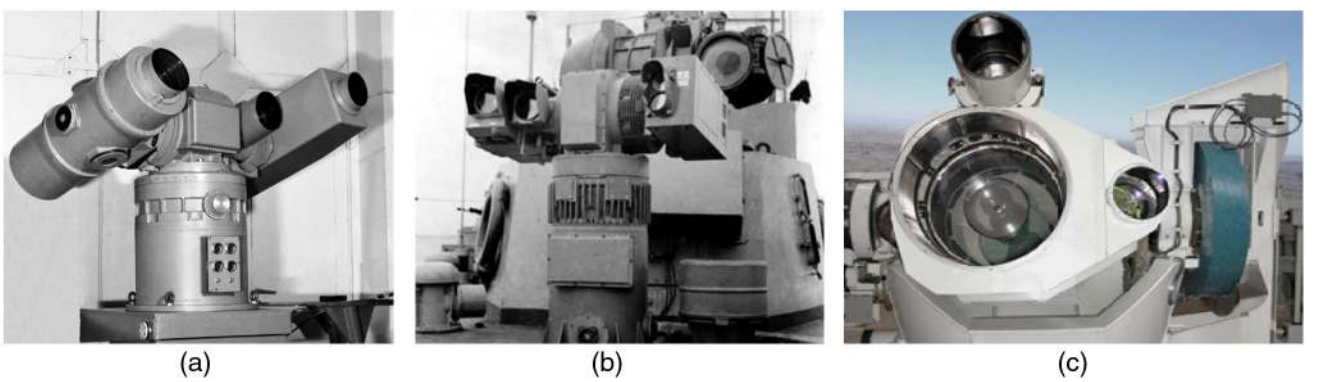

Fig. 6 FSU electro-optical systems with laser radars. (a) One of two on-deck devices of the Navy laser radar system (Kvant, Kiev), (b) multichannel CM with laser radar surveillance and fire control system (Kvant, Kiev), and (c) precision ranging and angular measurement system (Altai Optics-Laser Center).

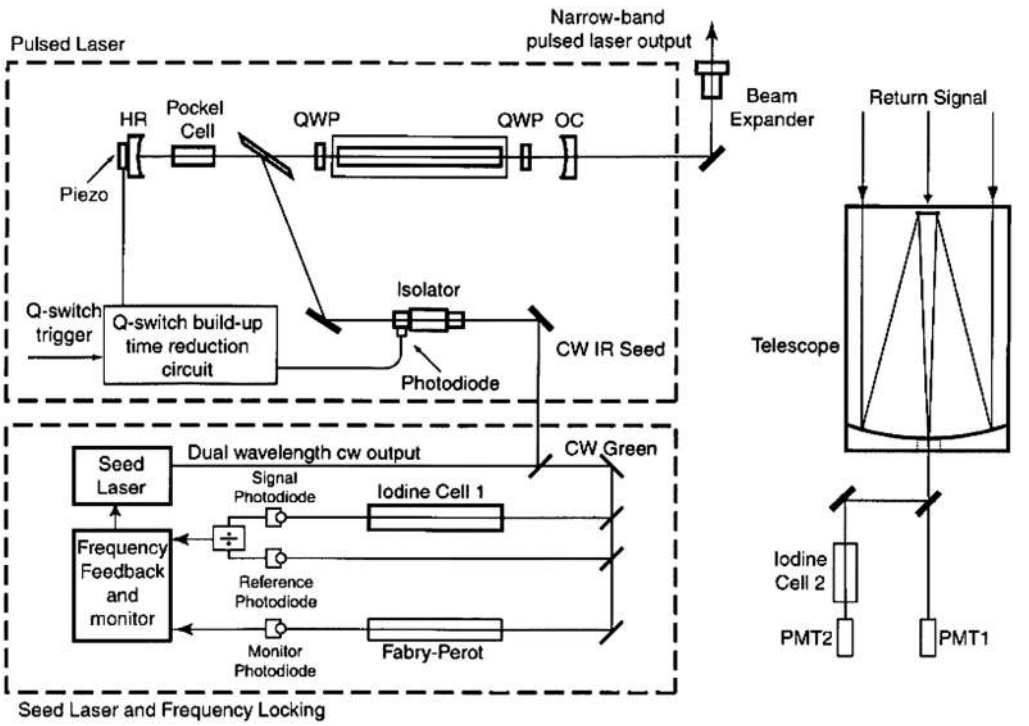

Fig. 7 Schematic diagram for injection-seeded Q-switched pulsed Nd:YAG laser transmitter.[26]

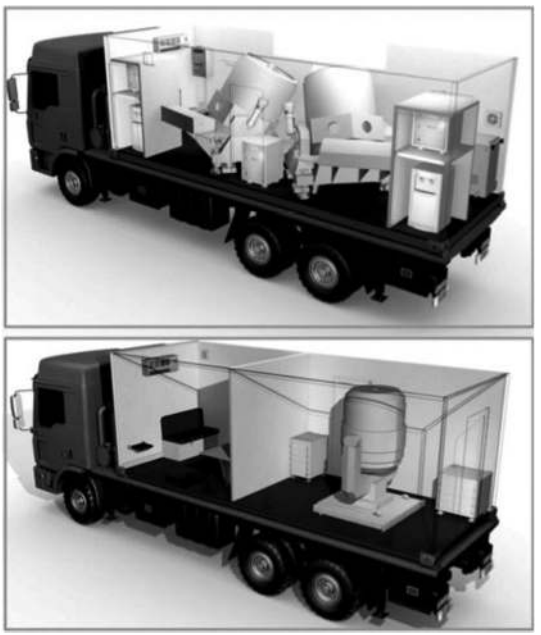

Fig. 8 Perspective view of two lidars.[28]

measure the amplitude (intensity) of the return laser signal. A typical application for coherent laser radar is velocity measurement, because by measuring phase, we can directly measure the Doppler frequency shift.

Airborne coherent laser radars have been used for ground imaging, obstacle warning, terrain following, as well as wind sensing including backscatter measurements. CLARA was a French-UK system developed for hard target (cables, ground surface, and so on) measurements.[35] This equipment followed successful trials of the "laser obstacle and cable unmasking system" pulsed CO_2 laser radar jointly developed by two groups within the former GEC Marconi. In another project, Société française d'équipements pour la navigation aérienne in France, a frequency-modulated CW (FMCW) laser radar was demonstrated for terrain following and terrain avoidance of combat aircraft.[36] The LATAS airborne lidar developed by RSRE was mainly used for true air speed and atmospheric backscatter measurement at 10.6 μm, but also demonstrated intensity imaging of natural terrain and manmade objects.[37]

Other applications using coherent laser radar have been precision navigation to a designated landing site on Earth or on extraterrestrial objects, and rendezvous and docking with orbiting spacecraft require accurate information on the vehicle relative velocity and altitude. A Doppler lidar was developed by NASA under the ALHAT project.[38] The lidar precision vector velocity data enabled the navigation system to continuously update the vehicle trajectory toward the landing site.

Figure 9 illustrates the configuration of an all-fiber lidar. Its waveform is generated from a very narrow linewidth fiber laser, is frequency modulated, and is directed through a single-mode fiber to a high-power fiber amplifier. The output of the fiber amplifier is split into three components in order to distribute the power to three optical channels corresponding to the velocity vector components (Fig. 10).

3.2 *Atmospheric Wind Sensing*

Wind sensing is a valuable application for coherent laser radars.[39] Measurements include various ground-based programs, such as local wind field measurement and wake vortex investigation at airfields (Fig. 11). Airborne systems are used to measure true airspeed, pressure error, wind shear warning, and to collect atmospheric backscattering over the

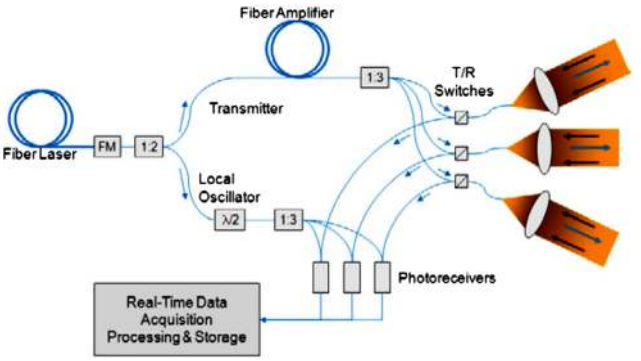

Fig. 9 Doppler lidar system configuration.

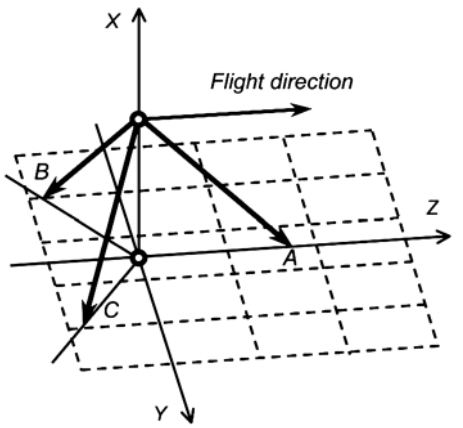

Fig. 10 Unit vectors describing the sensor geometry.

North and South Atlantic. In the 1990s, the European Space Energy supported a space-borne wind lidar in the Atmospheric Laser Doppler Instrument program. Pioneering wind lidar work in Europe was performed at RSRE (United Kingdom), DLR (Germany), and at the Laboratoire de Meteorologie Dynamique, Ecole Polytechnique (France). For a review on early coherent laser radar work in Europe, we refer to the paper by Vaughan et al.[40] In the book of Killinger and Mooradian (editors), there are several articles dedicated to the first coherent laser radars in the United States.[41]

Coherent Doppler lidar (CDL) appeared to be a useful instrument for atmospheric wind sensing, from ground, air, or space. CDLs observe large volumes of atmosphere with high spatial and temporal resolution, making these data important for many applications.

The first CDL was reported by Huffaker et al.[42] for wake vortex detection in 1970 using a 10.6-μm CW CO_2 laser. In the late 1990s, Mitsubishi Electric commercialized eye-safe compact fiber-based lidars and middle-range (8 km) wind lidars (Fig. 12), having developed a high power fiber amplifier of Er, Yb:glass with a 3.3-kW output power, 580-ns width, and repetition rate of 4 kHz.[43] Also, a ultra-long-range wind lidar exceeding 30 km was realized using this amplifier, with a range resolution of 300 m.[44] An all-fiber CDL was also developed based on a new concept of the automatic parameter control adaptive to atmospheric condition. These systems have been used in various industrial applications, such as meteorological monitoring, wind survey for wind power generation and aviation safety, and so on.

In the late 1990 and early 2000, Coherent Technologies, Inc. (CTI) led the charge to develop wind sensing, with sponsorship mostly from the Air Force and NASA. CTI also developed commercial products like the wind tracer. Multiple WindTracer systems have been deployed at airports and research facilities for monitoring the wind shear in the airport area and for study of aircraft wake vortices.

Another application for this technology has recently been the monitoring of winds for wind energy generating platforms. These units are placed on the tower and monitor the wind and turbulence for better operation of the wind power generators. Halo Photonics in United Kingdom and Leosphere in France offer these units commercially.

The US Air Force has interest in wind sensing for air drop, gun ship, and dropping dumb bombs. The flight version of ballistic winds was flown in a near prototype C-130 Pod System. It was 15 ft^3 and 1000 lbs. It used a solid-state, 15-mJ, 2-μm laser.

3.3 *Adding Range Finding to Velocity Measurements*

Coherent laser radars have the potential of adopting similar methods as in microwave radar to combine range finding with Doppler sensing. One of the concepts uses the principle of the FMCW signal. An example is the range finder developed at RSRE and described by Hulme et al.[45] The laser uses a few watts of output power. It is modulated by an acousto-optic modulator generating "chirp" pulses of the type familiar in microwave radar. Other examples are given in Refs. 46–48. At FOI, the systems were developed[49,50] using FMCW signals from CO_2 and semiconductor lasers.

3.4 *Vibrometry*

One of the attractive applications of the coherent laser radar is vibrometry based on the Doppler effect. Remote noncontact measurements offer potential for civil and military instrumentation. The vibrometers typically operate at 1.5, 2, or 10.6 μm. To get spatially resolved vibrational information, scanning and multibeam laser vibrometers are used. Reference 51 focused on applications in the field of defense and security, such as target classification and identification, including camouflaged or partly concealed targets, and the detection of buried land mines, with some examples of civil medium-range applications. The vibration spectrum of a target was acquired as an important and robust feature necessary for classification and identification purposes. The small target in Fig. 13(a) is an ordinary black rubber boat with an outboard engine. The boat is $\sim 4 \times 2 \times 2$ m^3. The range was $\sim$1 km. The diagram in the middle displays the frequency spectrum. The vibration frequencies originate from different parts of the target. To the right is the related spectrogram over 5 s.

Based on a spectrogram approach, vibration signatures were obtained from the LACE satellite in the course of ground-based laser radar measurements by using a coherent CO_2 laser.[52–54] The satellite was equipped with IR germanium retroreflectors on deployable/retractable booms to enhance ground-based IR laser radar measurements of on-orbit boom vibrations. The data were acquired during, and subsequent to, one of the maneuvers (boom retraction). They indicated the presence of a complex time-varying mode

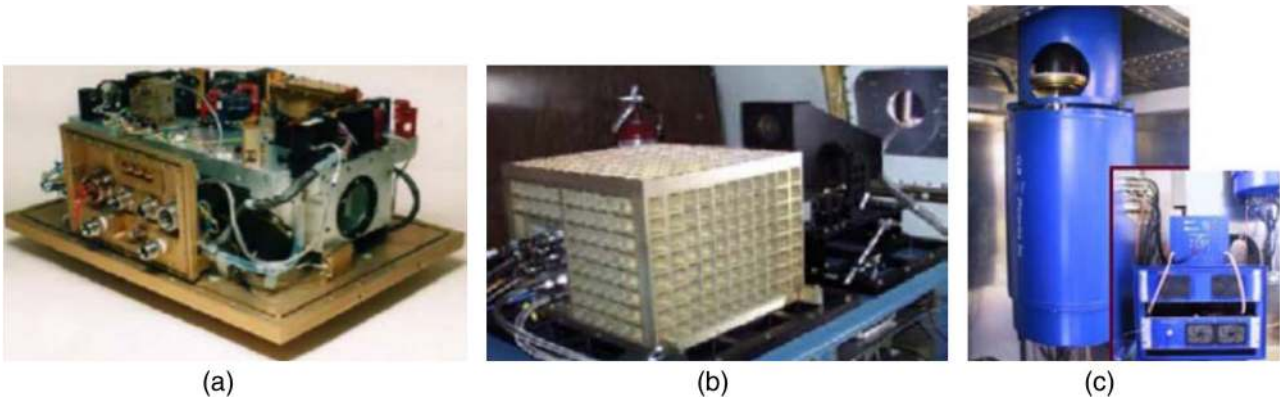

Fig. 11 Wind sensors: (a) NASA optical air turbulence sensor (2 μm, 1 mJ, 1 kHz, 5 cm aperture, chiller), (b) NASA ACLAIM turbulence warning (2 μm, 8 to 10 mJ, 100 Hz, 10 cm aperture, chiller), and (c) MAG-1A WindTracer (2 μm, 2 mJ, 500 Hz, 10 cm aperture, heat exchanger).

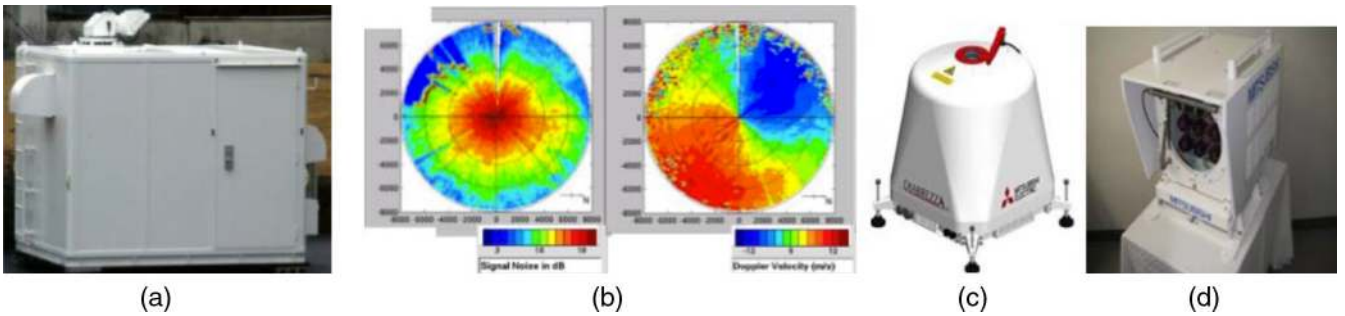

Fig. 12 (a) CDL, (b) displayed diagrams of signal noise and Doppler velocity, (c) all-fiber Doppler lidar system, and (d) its data display unit.

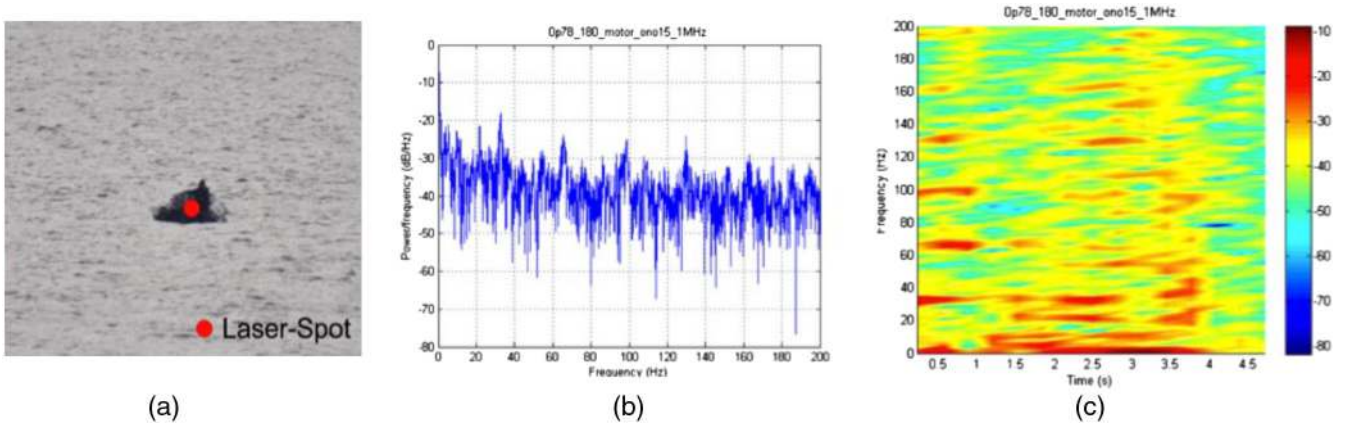

Fig. 13 Vibration measurements from a rubber boat. (a) Visible image with marked laser beam, (b) frequency spectrum of the velocity, and (c) frequency spectrum over time.

structure. The power spectra of vibrations are shown in a Doppler-time-intensity format in Fig. 14(b). Here, the power spectra are aligned and displayed along the vertical time axis. The horizontal axis corresponds to Doppler frequency (i.e., velocity).

Besides the CO_2 lasers at 10.6 μm, a number of solid-state laser sources based on neodymium at 1.06 μm, semiconductors or erbium fiber at 1.5 μm, and holmium at 2.1 μm have been used successfully as laser vibrometers. There are, however, often environmental conditions associated with poor visibility, turbulence, or high humidity, where it might be desirable to operate in the mid-IR band to improve system performance. Such conditions are not uncommon at low altitudes and in marine environments. Coherent laser radar systems in the mid-IR wavelength region can have advantages in low-altitude environments because they are less sensitive to scattering, turbulence, and humidity, which can affect shorter- or longer-wavelength systems. A monostatic coherent laser radar at 3.6 μm based on a single-frequency optical parametric oscillator was described in Ref. 55. It operated over short ranges outdoors, using two different stationary trucks with the motors running

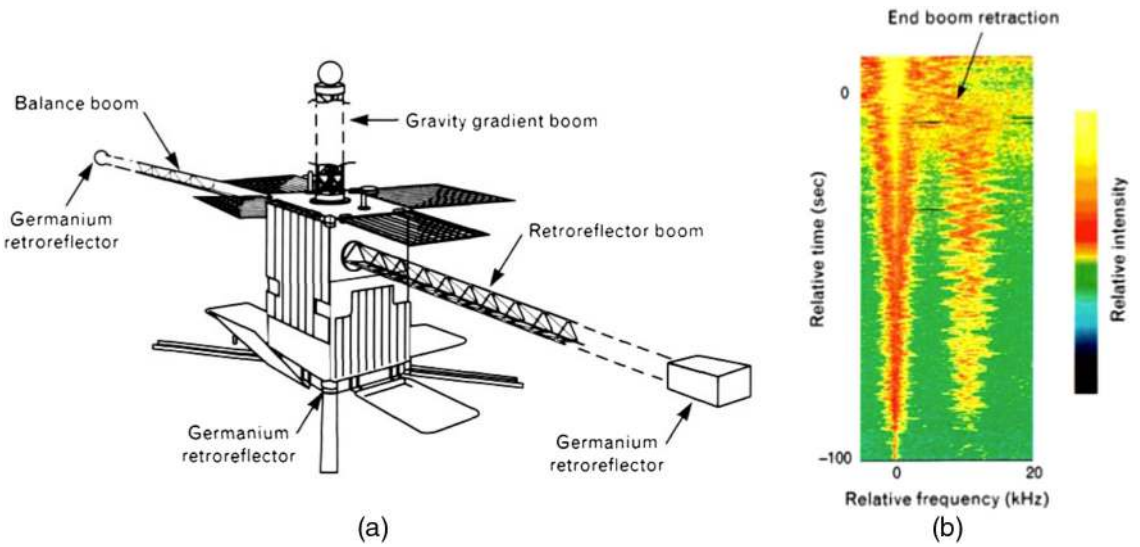

Fig. 14 (a) LACE satellite. Relative vibration was measured between the germanium retroreflector located on the satellite body and the retroreflector located on the retroreflector boom tip. (b) Doppler-time-intensity representation of data aligned to the peak return.

as targets. The system provided micro-Doppler measurements that were processed to give surface vibration spectra of the stationary, but running, trucks.

To get a spatial distribution of vibrations on the surface of the investigated object, a scanning vibrometer can be used. Scanning laser vibrometers allow analysis of the structure with a very fine spatial resolution, not modifying its dynamic behavior, decreasing the testing time if a large number of measurement points are requested. The problem of in-flight measurements was investigated using a scanning laser Doppler vibrometer to measure vibrations inside the cabin's mock-up of the Agusta A109MKII.[56] The whole area viewed was 430×315 mm^2. In the scanning tests, a 30×20 grid was used. The comparison was also made with the vibrograms measured when the vibrometer was placed outside the mock-up. Figure 15 is a summary of the tests at different resonances. They all refer to instantaneous amplitude of the velocity component at a certain frequency orthogonal to the surface with the bandwidth ± 10 Hz for the frequencies up to 1000 Hz and ± 30 Hz for the frequencies up to 5000 Hz. Vibration sensing was also examined for buried mine detection.[57]

4 Environmental Laser Radars (Lidars)

4.1 *Early Steps*

In parallel to military laser sensing, the laser radar research community started to search for applications in atmospheric and ocean sensing. For example, laser radar observations of the mesosphere were made using a ruby laser as early as 1963 by Fiocco and Smullin.[58] Spatial distribution of aerosols in the troposphere was reported by Collis et al.[59] In the United States, vertical water vapor distribution was studied[60] using a temperature tuned ruby laser; it was the first experiment using differential absorption lidar (DIAL). In Japan, a Mie scattering laser radar was first developed by utilizing a homemade Q-switched ruby laser. Basic relations were analyzed in 1968 on the scattering, extinction, and visibility by Inaba et al.[61] at Tohoku University. In the FSU, the atmosphere temperature was studied by Arshinov et al.[62] Laser sensing of the humidity profile of the atmosphere was studied by Zuev et al.[63] Examples of lidar systems[64,65] are shown in Fig. 16. As reported by Hu and Qiu,[66] the first Chinese atmospheric laser radar was completed in 1965. Since then, experimental studies were carried out to investigate

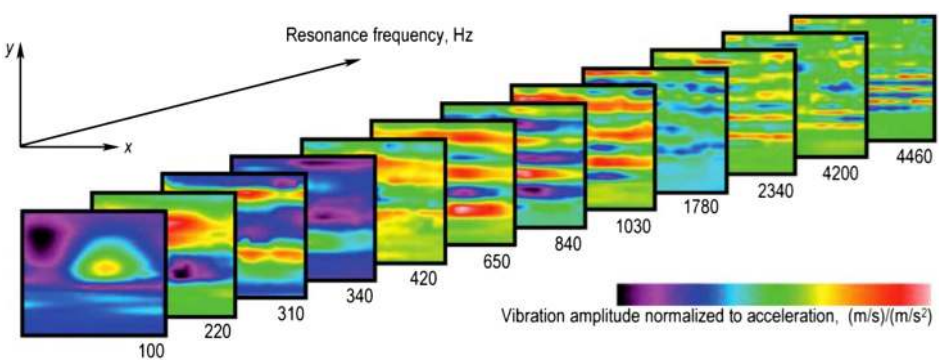

Fig. 15 Resonance vibration frequencies registered in the cabin of the helicopter mock-up.

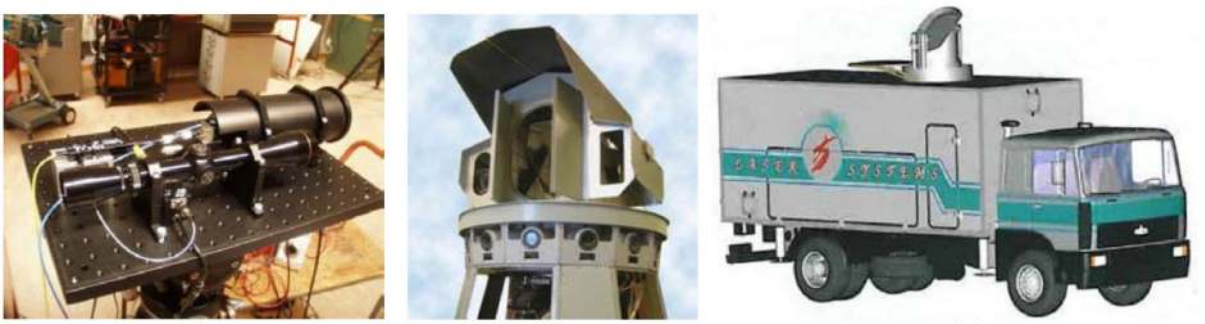

Fig. 16 Lidars for atmosphere investigation: (a) all-fiber coherent multifunctional CW laser radar for range, speed, vibration, and wind measurements at 1.55 μm (FOI, 2000), (b) Lidar automatic system for remote air pollution monitoring in large industrial areas (former Institute of Precision Instrumentation, Moscow), and (c) multifunctional lidar system (Astrofizika Corporation, Moscow).

stratospheric aerosol and volcanic cloud, stratospheric ozone profile, tropospheric aerosol (including smoke plume density, aerosol extinction coefficient, atmospheric turbulence), sodium layer and Rayleigh scattering in middle atmosphere, seawater temperature, oil slicks on sea surface, and so on. Numerous theoretical studies were also made. Svanberg[67] gives many examples of early laser radar monitoring of pollutants. Atmospheric and ocean laser radars involve all kinds of lasers and detectors depending on the goal of the laser radar. Possible goals might be aerosol or gas sensing, or ocean sensing, such as bottom profiling or water sensing (turbidity, plankton, and so on). The limited space in this paper does not allow us to go deeper into the atmospheric and ocean lidar development. Instead, we refer to the textbooks and reviews for further reading.[68,69] Reference can be made to two other books discussing the propagation of laser radiation in water medium.[70,71] Studies of the environmental laser radars in the FSU resulted in the seminal monographs on propagation of laser radiation in the atmosphere by Tatarskiy[72] and by Zuev.[73] They were followed by other monographs from the Tomsk scientific school.[74,75] Practical problems connected to the applications in meteorology were discussed in the book for meteorologists.[76] Achievements of the CW FM technologies are described in the book by Agishev.[77]

4.2 *Multiwavelength Lidars*

Penn State University[78,79] made significant progress in Raman laser radar. They enabled measurements of the optical and meteorological properties of the atmosphere based upon vibrational and rotational energy states of molecular species, such as water vapor and ozone, temperature, optical extinction, optical backscatter, multiwavelength extinction, extinction/backscatter ratio, aerosol layers, and cloud formation/dissipation (Fig. 17). An angular scattering technique enhances the information by measuring the scattering phase function for aerosols, including the polarization ratio of the scattering phase function, number density versus size, size distribution, identification of multicomponent aerosols, index of refraction, and so on. Multistatic aerosol laser radar and multiwavelength multistatic laser radars are good candidates for prospective studies.

4.3 *Laser Radar Sensing in China*

Studies of yellow sand storm events were one of the practical applications of Mie scattering laser radar in China, monitoring the transport of dust, aerosol extinction coefficient profiles, regional air pollutant transport, and the urban mixed layer.[80–82] In addition, Anhui Institute of Optics and Fine Mechanics (AIOFM) has joined national and international projects on lidar monitoring of the atmosphere.[83,84] These projects include the Asian Dust lidar observation NETwork,[85] Aeolian Dust Experiment on Climate impact, etc. A double wavelength polarization Mie laser radar was implemented,[86] and a 12-year observation of aerosol in Hefei was reported.[87]

The first Mie scattering laser radar was implemented to measure stratospheric aerosol in 1980s at the Institute of Atmospheric Physics (IAP). The stratospheric aerosol enhancement by volcanoes El Chichon (1982) and Pinatubo (1991) was monitored in Beijing. In the early 1990s, AIOFM started to develop Mie scattering lidar based on a Nd:YAG laser. A large amount of profile data of the Pinatubo volcanic cloud were obtained in Hefei and Beijing.[88]

In 1992, IAP developed a multiwavelength laser radar to observe stratosphere ozone and aerosols and the high altitude clouds. The laser radar used a XeCl excimer laser and a Nd:YAG laser, a 1-m diameter telescope, and multichannel detector. The Nd:YAG laser had outputs of 1 J, 300 mJ, and 150 mJ at 1064-, 532-, and 355-nm wavelength, respectively. The PRF was 10 Hz. The excimer laser had an output of 140 mJ at 308 nm and the PRF was 100 Hz.[89] In 1994, AIOFM also developed a laser radar using the second and third harmonics of Nd:YAG and an excimer laser for stratospheric ozone profile monitoring.[90] A DIAL for pollutant gas, such as SO_2, O_3, NO_2 observation, was developed in AIOFM.[91,92] A CH_4 and D_2 gas cell was pumped by the fourth harmonic of Nd:YAG.

The vibrational–rotational Raman laser radar was developed at Xi'an University of Technology.[93] A schematic diagram of the vibrational–rotational Raman laser radar is presented in Fig. 18. The system employs a pulsed Nd:YAG laser as a light source, operating at a frequency tripled wavelength of 354.7 nm with a 20-Hz repetition rate and an energy output of 250 mJ with a 9-ns pulse duration. Returned signals are collected with a 600-mm Newtonian telescope, and then coupled into a multimode optical fiber and guided

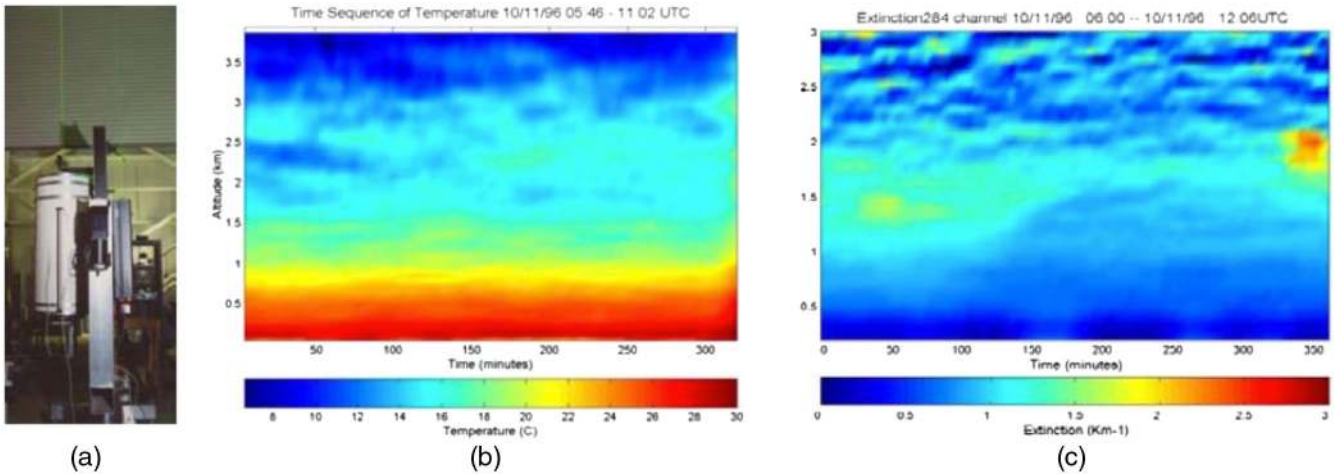

Fig. 17 (a) Lidar at the Pennsylvania State University and (b and c) dynamics of temperature and extinction.

into the spectroscopic box. The laser radar was used to measure profiles of water vapor mixing ratio by Raman scattering as well as the aerosol extinction coefficient by Mie scattering.[94,95] High accuracy temperature profiles can be achieved up to a height of 25 km.[96] The effective measurement for atmospheric water vapor can be achieved up to a height of 16 km.[97] Examples of extinction and temperature profiles are given in Fig. 18.

The first sodium laser radar for the middle atmosphere in China was developed in 1996 at Wuhan Institute of Physics and Mathematics.[98] Rayleigh and sodium lidar was developed by Wuhan University.[99] The laser radar transmits both in 532- and 589-nm wavelengths and detects Rayleigh backscattering, Raman signal of N_2 and H_2O, and sodium fluorescence. Similar sodium laser radars were also developed at the University of Science and Technology of China,[100] and Wuhan University.[101] Wuhan University developed an iron Boltzmann lidar to measure the mesopause temperature.[102] National Space Science Center developed a sodium fluorescence Doppler lidar to observe both temperature and wind.[103] At present, five laser radars (in Wuhan, Hefei, Qingdao, Beijing, and Hainan) are operating to observe the middle atmosphere.

4.4 *Laser Radar Sensing in Japan*

In Japan, a Raman scattering laser radar for sensing of air pollution over Japanese industrial areas was proposed by Inaba and Kobayashi[104] at Tohoku University. Raman scattering laser radars are shown in Fig. 19. A nitrogen molecular laser at ultraviolet 337.1-nm wavelength was developed for the Raman laser radar. Molecular vibrational Raman spectra of CO_2, O_2, N_2, and H_2O were observed in the clear air and it was shown for the first time that major air molecules could be separately detected. Also, various molecules, such as O_3, CO, CH_4, liquid and vapor H_2O, were identified from automobile exhaust gas in air. After this experiment, the mobile scanning Raman laser radar system was developed by Nakahara et al.[105] at Mitsubishi Electric Co. Ltd. using a Nd:YAG laser second harmonic beam at a wavelength

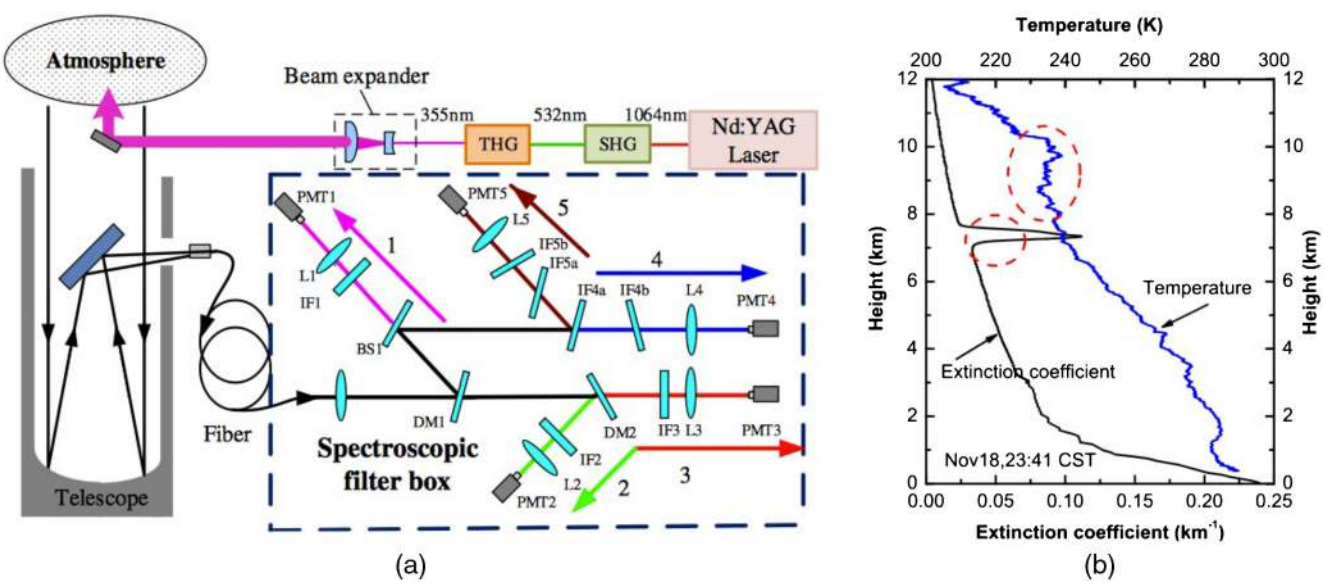

Fig. 18 (a) Vibration-rotational Raman lidar system developed at Xi'an University of Technology and (b) extinction and temperature profiles.

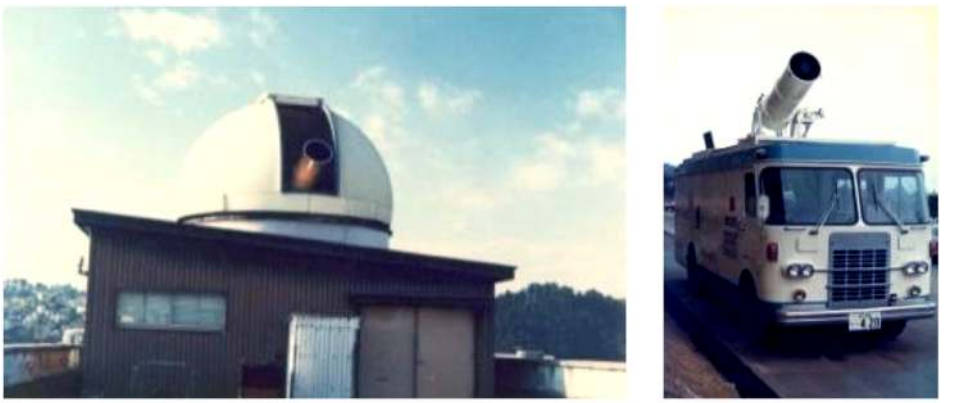

Fig. 19 (a) Early Raman scattering lidar systems: at the observatory of Tohoku University and (b) mobile scanning Raman lidar.

of 532 nm. It was shown that SO_2 molecules in stack effluent plume were detectable with 1000 ppm concentration sensitivity at the slant range of 220 m. The Raman laser radar was also used for humidity sensing by water vapor Raman spectroscopic detection and was gradually extended into sensing of extinction coefficients of atmospheric aerosols by simultaneous measurement of Mie and nitrogen Raman spectra.

After the demonstration of high sensitivity of resonant scattering laser radar in 1969,[106] several Na (sodium) resonant scattering lidars were developed and reported by Aruga et al.[107] at Tohoku University and by Nagasawa et al.[108] at Kyushu University.

Stratospheric ozone was measured by Uchino et al.[109] at Kyusyu University in 1978 employing a discharge-pumped XeCl laser at 308 nm wavelength based on the differential-absorption technique. In 1988, the Meteorological Research Institute developed a mobile laser radar for simultaneous measurements of ozone, temperature, and aerosols in the stratosphere.[110] They used three Stokes lines (276, 287, and 299 nm) of stimulated raman scattering from a carbon dioxide gas cell pumped by a Nd:YAG laser (266 nm).[111] The National Institute for Environmental Studies (NIES) also developed the same type of ozone DIAL.

To clarify the ozone loss mechanisms in the polar stratosphere known as the "ozone hole," a XeF excimer laser, with 200-mJ pulse-energy and 80-Hz repetition rate at 351- and 353-nm wavelengths, was developed. It was used in 1986 for observation of molecular density and temperature in altitude range of the middle atmosphere by T. Shibata et al. at the Kyushu University.[112]

To examine the potential of Mie scattering, a large scanning laser radar was built in 1979 at the National Institute for Environmental Studies, NIES, in Japan with a pulse energy of 400 mJ at 532 nm and repetition rate of 25 Hz (Fig. 20). The laser radar was used in various studies on Mie scattering for measuring the structure of the atmospheric boundary layer,[113,114] aerosol distribution, and optical characteristics.[115]

5 Imaging Laser Radars

5.1 *Early Laser Radar Imaging*

Imaging laser radars usually generate a 3-D point cloud of an area by measuring range and time-of-flight of laser waveforms at a large number of azimuth and elevation positions. To measure range at a large number of angular positions, scanners were initially used. More recently, detector arrays have become available, allowing flash imaging. In flash imaging, detector arrays are used to simultaneously obtain range data at multiple angular locations. Imaging laser radars can obtain reflectivity, spectral parameters, polarization, Doppler shift, and 3-D data. This breadth of data is why we refer to the rich laser radar phenomenology. Military and security applications include target recognition, target location, aim point selection, tracking, and weapon guidance. Military laser radar for imaging became of interest during the 1970s and 1980s. Important contributions were made by MIT/LL.[116] The Infrared Airborne Radar (IRAR) MIT/LL testbed was primarily an experimental target recognition system[117] capable of detecting and recognizing armored tactical vehicles in registered range and intensity images provided by a pulsed, infrared, CO_2 forward-looking laser radar that was carried either on a truck or aboard an aircraft.

Examples of images from MIT/LL are shown in Fig. 21. The left one is an IRAR CO_2 (10.59 μm) laser radar image of a bridge in which the range to each picture element is coded in color. The data collected in the original oblique view are transformed into an overhead view, as shown in the inset image. This rotation capability is one of the advantages of 3-D imaging. This view may be useful for missile seekers that use terrain features for targeting. Next, Doppler-velocity image was collected by a truck-transportable CO_2 laser radar. The Doppler shift of each of the ~16,000 pixels in the image was extracted by a surface acoustic-wave processor at a frame rate of 1 Hz. Velocity is mapped into color. The ability to sense moving parts on a vehicle provides a powerful means to discriminate targets from clutter. The next image made with a GaAs (0.85 μm) laser radar is an angle-angle-range image of a tank concealed by a camouflage net. The laser radar utilizes a high-accuracy, sinusoidal, amplitude-modulated waveform while observing the tank in a down-looking scenario. The camouflage net was readily gated out of the image to leave the tank image below the canopy. The far right image is a range-Doppler image of the LAGEOS satellite collected by the wideband CO_2 laser radar. This image was made with a bandwidth of 1 GHz. Doppler velocity resolution is ~30 cm/s. Color in the image represents relative signal amplitude.

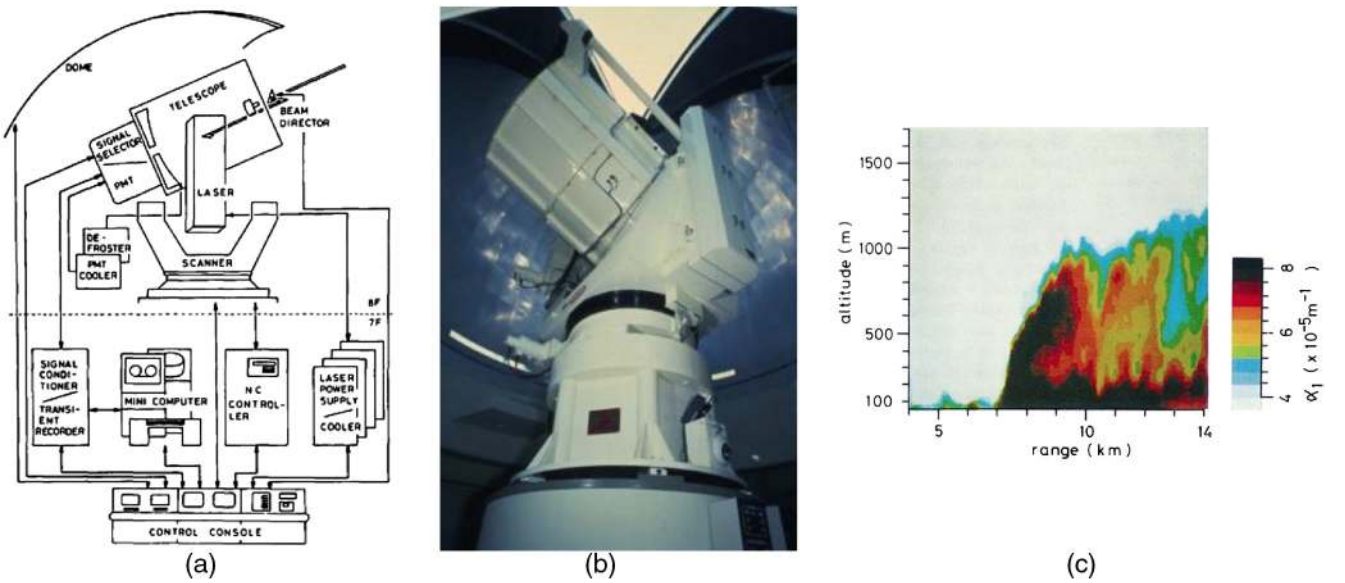

Fig. 20 Large scanning lidar system (NIES): (a) schematic diagram, (b) photo of the lidar, and (c) structure of sea breeze front.

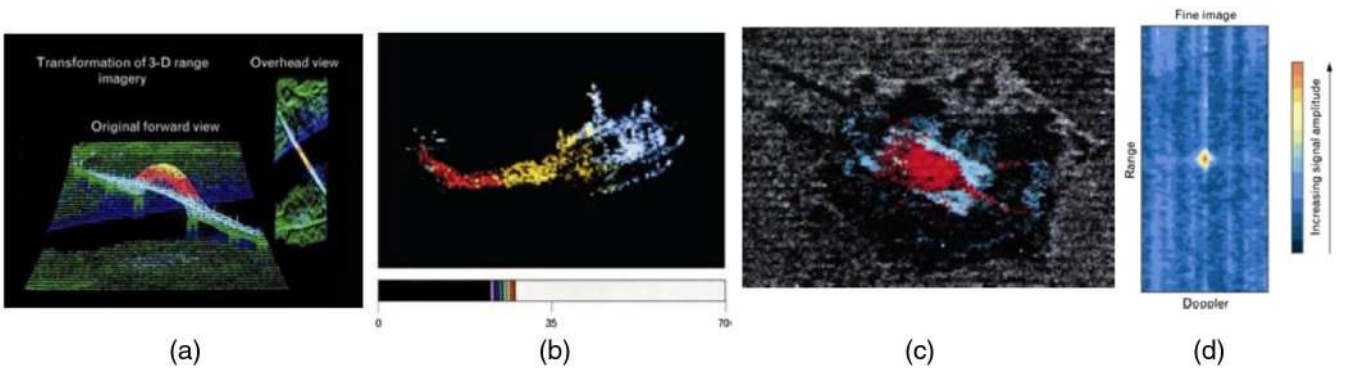

Fig. 21 Images from MIT/LL laser radar systems: (a) CO_2 laser-radar images of a bridge, (b) Doppler-velocity image of a UH-1, (c) laser-radar image of a tank concealed by a camouflage net, and (d) range-Doppler image of the LAGEOS satellite collected by the wideband CO_2 laser radar at Firepond.

Early laser imaging radars were performed at Raytheon.[118,119] One example was the triservice laser radar containing a CO_2 15-W waveguide laser and a galvanometer scanner, a TV and an InSb IR camera. This system was used in numerous campaigns for evaluation of imaging laser radar technology. In parallel with the coherent laser radars, scanning direct detection laser radars became more interesting due to somewhat better performance in intensity recording (less speckle issues) and better range accuracy and resolution. A US example of scanning direct detecting laser radars in the early 1990s was the Hercules Defense Electronic Systems laser radar,[120] which was operated at both the 1.047- and 1.319-μm wavelengths of Nd:YLF. The 1.319-μm transition was reported to yield about 6 to 8 dB less peak power than the 1.047-μm transition, but offers the advantage of significantly enhanced eye safety characteristics. Another example is the Fibertek Helicopter Laser Radar (HLR) system,[121] which was designed primarily for terrain following and wire obstacle avoidance. The HLR system generates eye-safe 1.54-μm radiation using a Nd:YLF transmitter and a KTP OPO. The Nd:YLF laser generates 5-ns pulses at up to 15-kHz PRF. Average power at 1.54 μm was ~1.0 W.

Early imaging laser radar work in Europe included coherent CO_2 systems in France[122] and Sweden.[123–125] Figure 22 shows an example of a multifunctional coherent CO_2 laser radar system developed in the 1980s at FOI. In this system, a pulsed laser radar with a programmable transmitter was built to study the combined capability of Doppler and range imaging. A new technique was investigated[126] for terrain segmentation based on range data. The basis of the approach was to model the range values obtained from horizontal and vertical scans as a piecewise constant (or linear) signal in random noise.

5.2 *Range-Gated Imaging Programs*

The 2-D range-gated imaging programs started in the 1990s. The US Air Force had a program called ERASER.[8] The idea was to use the designator laser already on an aircraft to enhance recognition range. A designator has a shorter wavelength then a thermal imager and can provide better

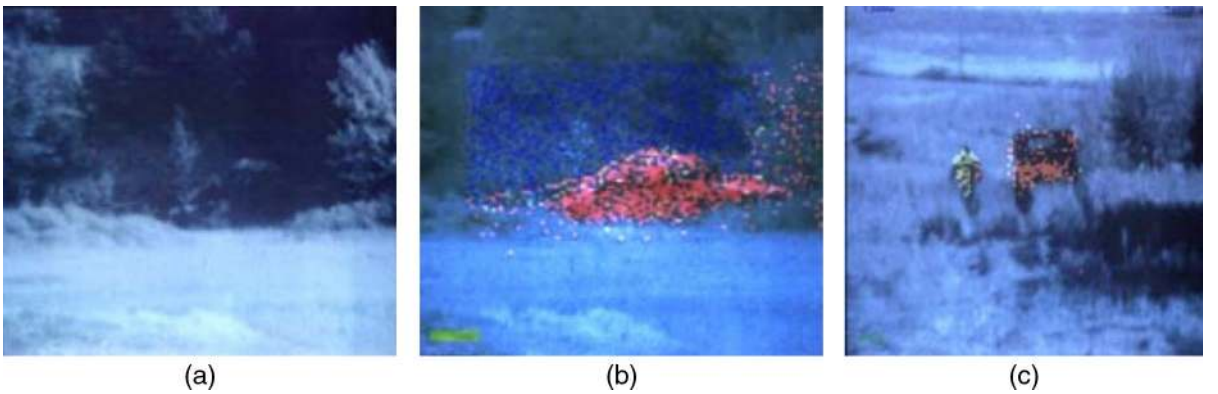

Fig. 22 Imaging range and velocity with pulsed CO_2 laser radar (FOI). (a) TV image of a hidden tank, (b) TV image with a range image overlay from a coherent CO_2 laser radar, and (c) "Doppler pixels" overlayed on a TV image.

diffraction-limited angle resolution and longer ID ranges than a thermal camera. A laser-based system also provides its own illumination, so it is not as subject to time of day variations, such as cross over in thermal imaging. Range-gated imaging also gives a very good target to background contrast, especially if the target is seen in a silhouette mode.

A US Army study picked up on the US Air Force initiated gated 2-D imaging work and did modeling and testing of the prototype equipment.[127] The performance of range-gated systems is limited by the sensor parameters as well as the target- and atmospheric-induced speckles, beam wander, and image dancing,[128,129] because 2-D imagers are usually direct detection speckles that can be mitigated by using a wider laser bandwidth to speckle average. Close to the range limit, the shot noise restricts the image quality. Frame to frame integration is often used for reducing the scintillation and target speckle effects in which case the image dancing and atmospheric coherence time become of importance. Range resolved 3-D images can be reconstructed from a series of sliding gated imagery.[130]

Gated active 2-D imaging was studied by the major defense research laboratories. An overview of the range-gated imaging at FOI including performance modeling was recently published at SPIE.[131] The work included diode laser-gated systems, 532-nm systems, and lately an eye safe 1.5 μm using the Intevac tube technology. In later publications,[132] FOI and IOSB published the results of their studies both of mono- and bistatic configurations with 1.5-μm range-gated systems. Examples of range-gated applications for marine environments include identification of small surface vessels[133–135] and divers. Gated viewing for underwater imaging has been tested for a long time[136–138] and recently has been used with range gating with subcentimeter accuracy.[139] Scanning systems were studied for the detection of underwater objects in front of ships.[140]

5.3 *3-D Laser Radars*

Development of 3-D flash laser radars with intensity and range information in each pixel obtained from one illuminating pulse encouraged the research of the focal plane array detectors. APD arrays based on HdCdTe are of high interest and are under development by several groups, such as Raytheon,[141] DRS, Sofradir/Leti,[142] and Selex.[143] Beside linear APD arrays, a lot of attention is paid to photon counting detectors of the Geiger-mode APDs (GMAPDs). MIT/LL has pioneered development of GMAPDs for such laser radar programs as Jigsaw.[144,145] Jigsaw 3-D laser radars have a poke through capability to look through the gaps in camouflage and between the leaves in vegetation. MIT/LL developed a laser radar, which produced high-resolution 3-D images using short laser pulses and a focal-plane array of 32×32 GMAPDs with independent digital time-of-flight counting circuits at each pixel.[146,147] Figure 23 shows an example of the Jigsaw results. A target under trees can be seen after "range cropping" of the generated 3-D point cloud from the laser radar.

In 2010, a new application of 3-D laser radar was demonstrated for play stations. It was the first-generation Kinect, a motion sensing device, where the distance was determined using the triangulation principle. In 2012, a Kinect version for Windows was released, based on time-of-flight principle. Its sensors measure the lock-in phase differences between emitted and received signals. Near-infrared light from LEDs is modulated by a sine (or any other periodic) function. Each pixel of the sensor samples the amount of light reflected by the scene four times at equal intervals for every period, which allows for the parallel measurement of its phase. This phase demodulation technique is commonly known as "four-bucket" sampling and it permits to calculate the distance to the object. As a sensor, a CMOS chip is used consisting of the so-called smart pixels, each measuring individual distance to the observed scene. The number of pixels in the images is 176×144 in Swissranger SR3000 and SR4000 cameras and 204×204 in PMD CamCube camera. For further reading, we recommend to see Ref. 148.

Foliage poke through has also been studied in other labs. Grönwall et al.[149] proposed a sequential approach for detection and recognition of manmade objects in natural forest environments using data from laser-based 3-D sensors. Armbruster[150] discusses the exploitation of range imagery for examples drawn from the fields of helicopter obstacle avoidance, object detection in surveillance applications, object recognition at high range, multiobject tracking, and object reidentification in range image sequences. He argues that automatic target recognition (ATR) performance of objects detected by 3-D laser radars can exceed not only the 2-D ATR but also that for human vision.

Another US program was the SPI 3-D program[151] to "develop and demonstrate the ability to provide precision

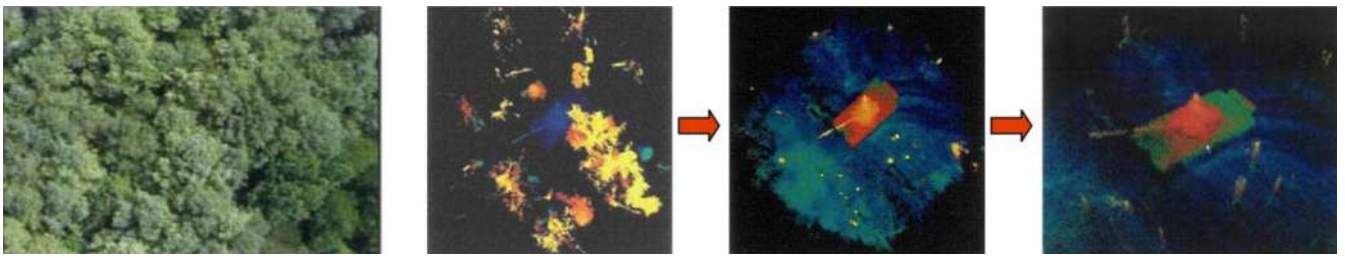

Fig. 23 Example of data from the Jigsaw detecting a tank target under trees.

geolocation of ground targets combined with high-resolution 3-D imagery at useful standoff ranges." These dual capabilities were provided using a sensor package composed of commercially available components. It was capable of providing "optical quality precision at radar standoff ranges" and had the ability to overcome limited weapons effects obscuration and penetrate moderate foliage.

5.4 *Imaging for Weapon Guidance*

Imaging laser radars can extend laser weapon guidance capability in a semiactive or beam riding mode. The drawback is an increased complexity of having the laser as a part of the seeker. Scanning laser radars have been intensely studied in the United States for missile applications. Target detection and homing were also studied for air to air seekers, and in space for the SDI program. The largest investments in laser radar seeker technology have been made for air to ground seekers. The Low Cost Autonomous Attack System (LOCAAS) was a demonstrator program[152] driven by the Air Force (Eglin Florida). The AFRL's LOCAAS program terminated in mid-2006 without going to production. The seeker was based on scanning laser radar generating 3-D imagery of the targets with ATR and aim point selection built into the system. Loitering Attack Missile[153] was a project within the US Forward Combat System relying on the laser radar technology developed for LOCAAS. The paper from Andressen et al.[154] gives some insight to this technology.

5.5 *Obstacle Avoidance Applications*

In Europe, interest in imaging laser radar seeker technology was more limited compared to the United States. One example of an operational obstacle avoidance system for helicopters is the German Hellas system[155] developed by EADS. The Hellas system was designed to warn pilots of obstacles in due time and to detect thin wires up to 1 km from the platform. It also has a brown-out recovery system. During the take-off and landing, helicopters can encounter serious brown-out or white-out problems in dusty, sandy, and snowy areas as the downwash of the rotor blades creates dust clouds around the helicopter. With the help of laser radar, an augmented enhanced synthetic vision of the landing area with surroundings is provided to the pilot based on range image data as well as on the altimetry and inertial reference information.

Other laser radar obstacle avoidance systems were developed in Israel and in the United States. The 3-D laser radar imaging has potential for many other applications including robotics, terrain visualization, augmented vision, reconnaissance, and so on. Different types of the 3-D laser sensors were proposed and implemented.[156–158] To minimize the transmitted energy, a pulsed 3-D laser sensor with 2-D scanning of the transmitting beam and a scanless receiver was proposed by Mitsubishi Electric Corporation.[159] The system configuration is shown in Fig. 24. The laser is a 1.5-μm pulsed fiber laser with pulse energy of 2 μJ and duration of 10 ns. The beam diameter of the collimated beam is about 1 mm. The aperture diameter of the receiving optics is 15 mm. The FOV of the receiver is about 6×6 deg. The signal processor generates an intensity image, a range image, and consequently, a 3-D image by combining with angle information for each pixel. To enable the system to obtain correct 3-D images, the processing includes a peak detection flag indicating whether the range and intensity detector recognizes the received signal or not.

5.6 *Flash Imaging Laser Radars*

Much of the imaging laser radar research today is centered on flash imaging. The technology is so far based mainly on 2-D range-gated imaging. The application is mostly targeting, i.e., the recognition of targets at longer ranges than a cooperating IR camera can provide, thus enabling a longer stand-off range for weapon release. Other applications for flash imaging are threat and surveillance/mapping systems combining 3-D focal plane technology and scanning (cf. the Jigsaw system mentioned above).

Figure 25 shows an airborne flash laser radar developed by Northrop Grumman Aerospace Systems.[160] The "flash" system had a 128×128 pixel array with a read out and integration circuit (ROIC) capable of storing an image every 0.5 ns. The ROIC captures 20 time lapsed images for each pulse. This can provide a profile in range at each angular position. These time lapsed images are then used to calculate the range estimates of the target area. It used a flashlamp pumped Nd:YAG OPO at 1.57 μm, with 50 mJ per pulse, a 6.7-ns pulse width, and a 30-Hz frame rate. At each 2-D pixel location, we have 20 range positions measurements, separated by 2.2 ns in range.

Processing for laser-gated viewing was developed by TNO Defence, Security and Safety (The Netherlands),[161] based on Intevac Livar 4000 laser-gated viewer (Fig. 26). The 1.5 μm eye safe laser was used and the EBCMOS camera for gated viewing (minimum gate shift: 1.0 m, minimum gate width: 20 m).

5.7 *Synthetic Aperture Laser Radars*

Synthetic aperture radars (SARs) are a mature field that was developed to reconstruct microwave images of high resolution by use of antennas of reasonable size. Their principle

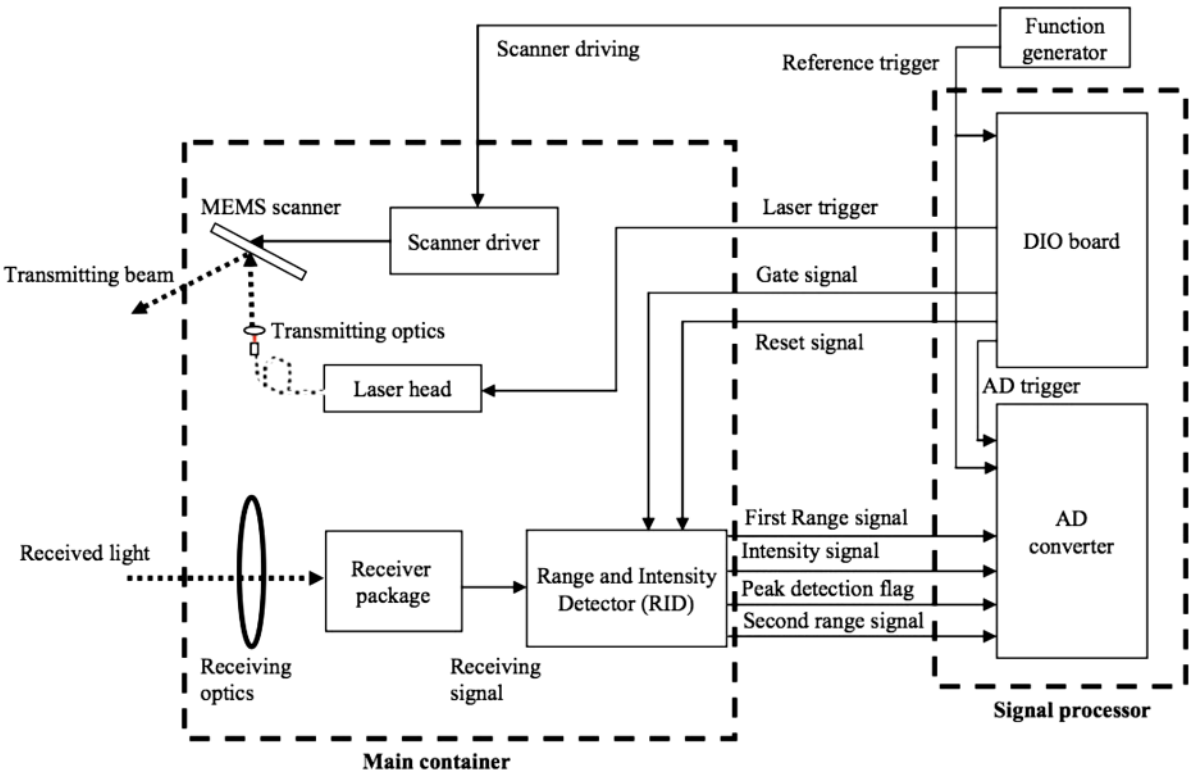

Fig. 24 Obstacle avoidance systems (Mitsubishi Electric Corporation).

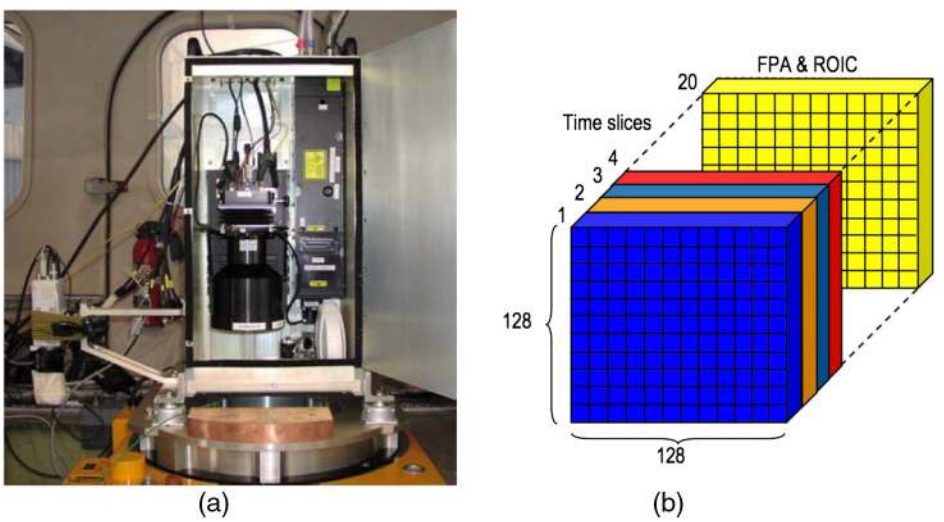

Fig. 25 Airborne flash laser radar developed by Northrop Grumman Aerospace Systems: (a) general view and (b) principle explanation.

is based on accumulating field information as the radar moves with respect to the target. A large area of pupil plane full-field information is then available. For a microwave radar the pupil plane field information allows to simulate a synthetic aperture that is kilometers long in one direction. Because field information contains both phase and intensity, we can Fourier transform this large pupil plane image to develop a high angle resolution image in the dimension with the long synthetic aperture. If the SAR has a high bandwidth, it can also provide high range resolution. A SAR, therefore, can provide a high angle resolution in one dimension and high range resolution in a second dimension, providing a high resolution image. Thus, the SAR technique is applicable when there is a relative transverse motion between the radar and the target, with the resolution improvement accomplished by increasing the effective aperture dimension in the direction of motion. SARs operate at microwave and millimeter wavelengths and are extensively used to improve far-field spatial resolution over that provided by conventional diffraction-limited radars. Because microwave radars have limited real beam resolution, there was a large incentive to develop SAR; microwave wavelengths

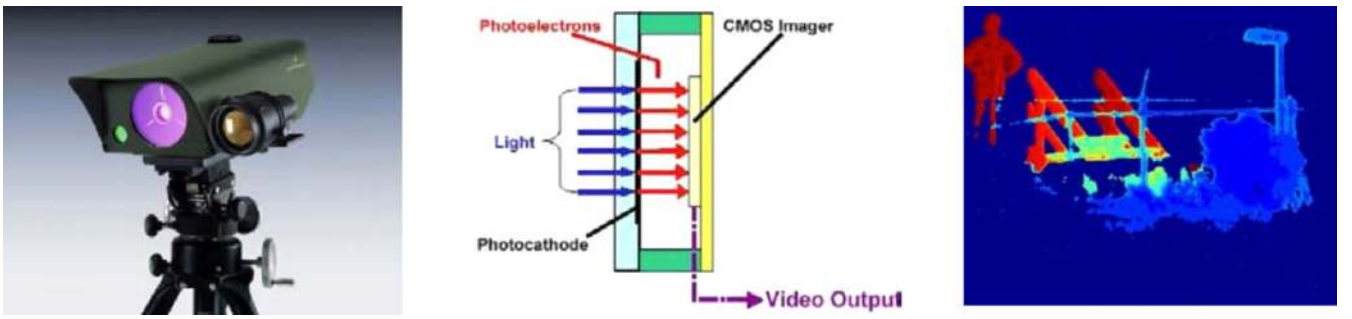

Fig. 26 Laser-gated viewing using Intevac Livar 4000 laser-gated viewer.

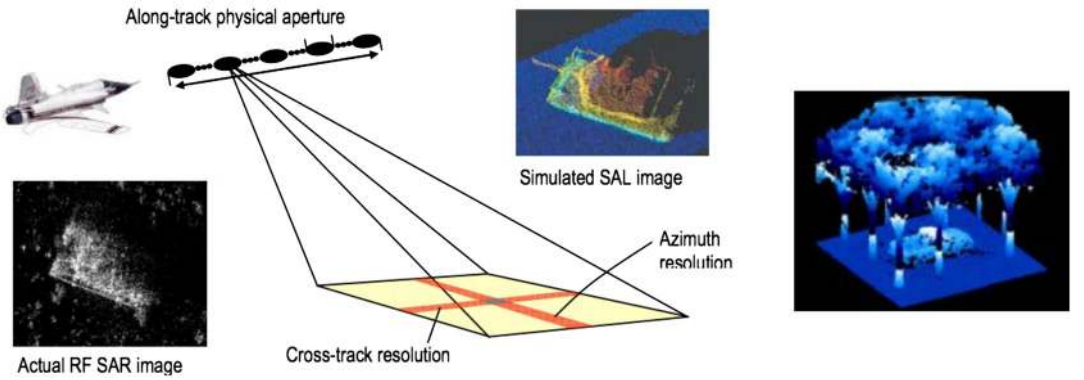

Fig. 27 Left: Principles of SAL radar. Right: processed SAL data, observing a truck through foliage. Information from four separate views is combined in this image (Northrop Grumman).

are also relatively large, allowing motion compensation to a fraction of a wavelength.

This technique was extended to the optical/infrared wavelengths with CO_2 laser sources,[162,163] and Nd:YAG lasers.[164,165] Because the difference in wavelength synthetic apertures can be much smaller at optical wavelengths, motion compensation must still compensate for any phase variations more than a fraction of a wavelength. If your wavelength is 3 cm, as in SAR, you must compensate for changes down to <3 mm. If your wavelength is 10 μm, you will need to compensate for changes <1 μm, and for a 1-μm laser radar, you will need to compensate for changes <0.1 μm. Feasibility studies continued since those initial investigations into synthetic aperture lidar, synthetic aperture laser (SAL) without interruption.[166–168] High resolution capability of an SAL can be used as an advantage not only for long-range applications (like space based imaging, for example) but also for short ranges if very high angular resolution is required. Examples of high resolution SAL imagery are shown in Fig 27. Because SAL focusing can be controlled by adjusting the assumed range in the pulse-compression filter, targets with range variations can be imaged with no degradation in along-track resolution. An example of such a short-range application is product quality control when the object has a varying surface relief.

6 Mapping Laser Radars

6.1 *Terrain Mapping*

Scanning laser radar systems are well established for terrain mapping and depth sounding. The civilian market has been leading this field for the last 20 years. Both space and airborne laser radar systems, as well as terrestrial laser radars, have been developed by several different vendors. The large number of publications and applications, as well as the rapid development of hardware, shows the large interest in this technology. A book giving a good overview of topographic laser scanning techniques was published by Shan and Toth.[169]

Many military applications coincide with the civilian ones. The major difference is found in the way data is processed and used. Military systems often have a higher need for area coverage, rate and/or spatial resolution, and they may have to work at higher altitudes and during the night time, and be more covert. Military mapping systems may also have the need for multifunction operation. Tactical mapping can be combined with surveillance and targeting capabilities. There is also a growing trend for military laser radar systems to operate from unmanned platforms [like unmanned ground vehicle (UGV), e.g., an autonomous car; unmanned aerial vehicle (UAV), commonly known as a "drone," autonomous underwater vehicle, for underwater operation) stressing the demand for low size, weight, and power consumption.

Wide area airborne mapping systems using conventional scanning and linear APDs have been developed by several companies (Optech/Teledyne, Riegl, Leica). These can fly up to 5- to 6-km altitude and have PRF up to 1 MHz. Recent trends are to make the systems small and compact as well as to combine laser scanning with digital and hyperspectral cameras. An example of a compact system is the Dragon Eye developed by AHAB[170] in Sweden (now Leica GeoSystems). It has a laser PRF up to 1 MHz and operates up to 15,600 m in altitude. The sensor head weighs 37 kg and the control unit weighs 53 kg.

Fig. 28 Example of a 3-D urban data collection using a Geiger mode lidar. From Harris Corporation web page.

GMAPD photon counting technology enables even faster data collection. It stems from military development by the US Air Force and DARPA. The sensor offered by Harris Corporation[171] is claimed to allow for larger area mapping than has been possible up till now, and to collect data up to 10 times faster, and with 10 times higher resolution, than with linear lidar sensors. The Harris sensor is a flash laser radar using a larger GMAPD focal plane array. Figure 28 shows imagery from this 3D mapping laser radar.

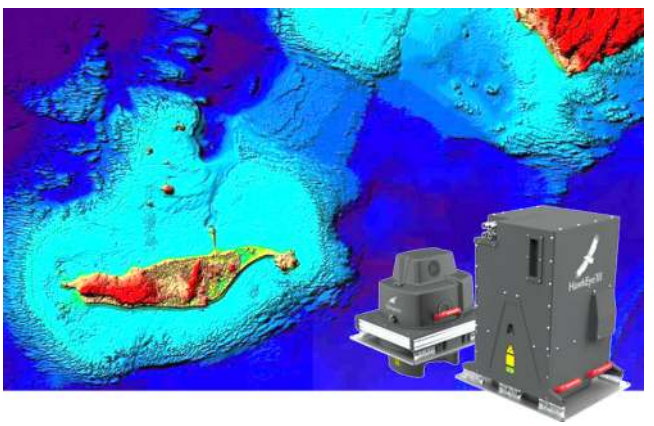

Fig. 29 Example of a lidar bathymetry system (Hawk Eye III from Leica Geosystems). The green to blue color is indicative of the water depth.

Laser scanners are used on UGVs for navigation and obstacle avoidance. The most widespread demonstration of the success of laser scanners was for the UGV112, where laser scanners were the key sensors. Systems from Teledyne Optech[172] and Velodyne Lidar[173] are the examples of commercial road mapping laser radars with many potential military applications (for example, generation of synthetic environments, detection of improvised explosive devices, and so on). The accuracy is said to be on the order of centimeters at a maximum range of 100 to 250 m. Measurement rates are found between 1 and 2 million points per second. This allows a 6-cm point spacing at 10-m range for a vehicle velocity 43 km/h.

Vehicle borne laser radar is becoming a very important sensor for self-driving cars. This may be the first widespread commercial application of laser radar technology. It will force the technology to be small and compact at a cost of a few hundred dollars per laser radar.

6.2 *Laser-Based Bathymetry*

Airborne laser bathymetry or hydrography is a technique for measuring the depths of relatively shallow coastal waters.[174] Typical applications include bathymetric surveys of federal navigation channels, large offshore areas, ports and harbors, shore protection projects, such as jetties and breakwaters, coral reefs, beaches, shorelines, and dredge disposal sites.[175,176] Topographic surveys above the water surface can be conducted simultaneously. Data can be acquired for storm surge modeling and for sand monitoring as a local resource. In a review paper,[177] hardware and software design philosophy is discussed in line with critical design considerations and a history of airborne lidar bathymetry development. Fig. 29 shows an example of bathymetry laser radar.

Examples of countries which have developed and used laser radar bathymetry include the United States, Australia, Sweden, Canada, and Russia. In 1990s, systems became operational in Australia (LADS[178]), the United States (SHOALS[179]) and Sweden (Hawk Eye[180]). The practical depth range for bottom charting is about 3 Secchi depths, i.e., 5 to 40 m in coastal waters.

7 Laser Microradars

7.1 *Optical Coherence Tomography*

The technique that became known as OCT[181] is a combination of time-of-flight measurement and interferometry. It was implemented using a Michelson interferometer by replacing of one of the mirrors with the object under test (Fig. 30).

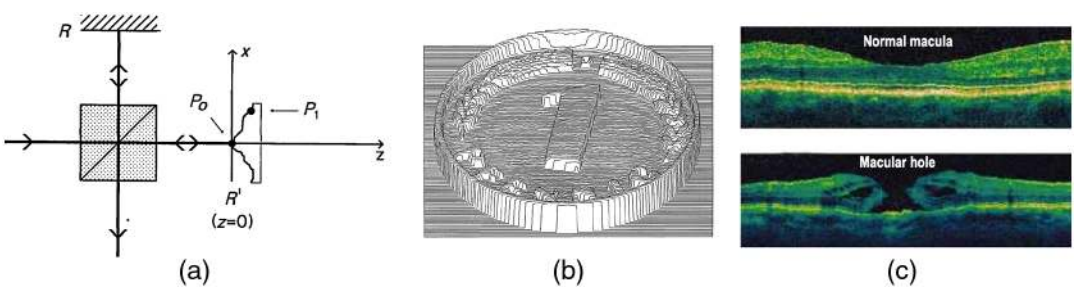

Fig. 30 (a) Basic setup of an optical microradar, (b) 3-D reconstruction of a coin image, and (c) eye bottom tomograms.

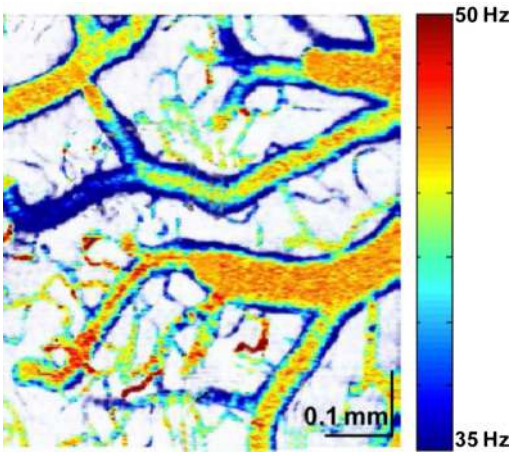

Fig. 31 Capillary velocity map.

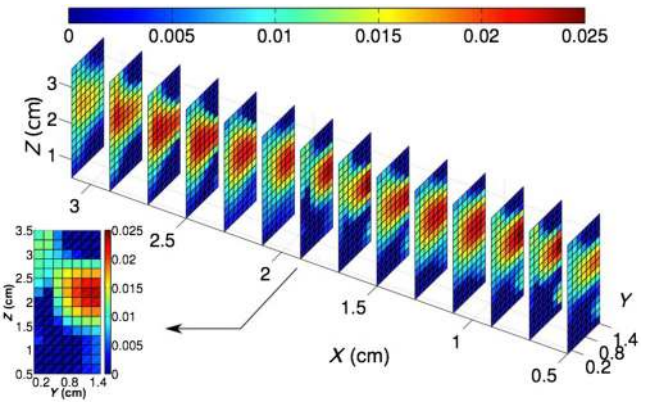

Fig. 32 Slices of flow velocity distribution.

A light source with short coherence length is used; therefore, a more correct term would be optical low-coherence tomography. The reference mirror, located at plane R, and the object plane are imaged onto a detector, which is focused onto plane R'. Planes R and R' are the same distance from the light source.

The image of an object is superimposed with a reference wave. Interference can be locally observed, where the light paths from the reference and the object are approximately equal. The measurement is based on interference. Because of the short coherence length, the interference takes place only within those speckles that correspond to the surface elements close to the plane R'. These regions are detected and stored, while the object is moved slowly along the z axis. In the same manner, the reference mirror can be movable when the object is unmoved. An example of a profile reconstructed by this technique using additional (x, y) scanning is presented in Fig. 31, which shows a coin.

Placing a human eye in the plane R' as an object to study, moving the plane R in axial direction z, one can get the profile of backscatter from the tissues and surfaces of the eye. Providing scanning in $x - y$ directions, a 3-D image can be reconstructed [Fig. 30(c)]. Hundreds of publications appeared in the last decades reporting on numerous modifications of the OCT and applications in different fields, especially in medicine: structure of the eye, 3-D imaging of blood vessels, blood flow in the vessels, and not only in ophthalmology but also in cardiovascular studies, cranial vascularization, and so on. There is no space within our short article to embrace all variants of OCT and of its application, so we address the readers to the encyclopedic-style books.[182–184]

7.2 *Capillary Velocimetry*

To demonstrate applications of the OCT capillary velocimetry in cerebrovascular research, a 1310-nm spectral/Fourier domain OCT microscope was used for *in vivo* imaging of the rat cortex.[185] The light source consisted of two super luminescent diodes yielding a spectral bandwidth of 170 nm. The axial (depth) and transverse resolution was 3.6 μm in tissue, full-width-at-half-maximum, and the imaging speed was 47,000 axial scans per second (17.3-μs exposure time), achieved by an InGaAs line scan camera. Capillary velocimetry and its imaging were performed during a hypercapnic challenge in a rat. An example of such imaging is given in Fig. 31.

Another tomographic method based on laser speckle contrast was introduced[186] that allows the reconstruction of a 3-D distribution of blood flow in deep tissues. The experimental set up uses a temperature controlled continuous laser diode (785 nm, 90 mW) to probe the sample. A pair of galvo-controlled mirrors is used to scan the laser point source. The light source is focused on the bottom of the sample and the produced speckle patterns are imaged from the top with a monochrome CMOS camera, with exposure time of 1 ms. The horizontal field-of-view is about 4 cm, the pixel diameter is 3×10^{-4} cm. The laser was set in every position during 0.5 s to acquire 35 intensity images. An example of a 3-D slice plot of the reconstructed flow velocity for original velocity of 3.18 cm/s is shown in Fig. 32.

7.3 *Wavefront Sensing*

As a response to the development of vision correction techniques, Molebny et al. in 1996–1998 developed three types of instruments for measuring the refraction nonhomogeneity of the human eye: single-beam direct detection ray tracing,[187] double-beam coherent ray tracing,[188] and Hartmann–Shack sensing with holographic lenslet array.[189] Single-beam ray tracing aberrometry is based on laser radar principle: laser beam is projected into the eye in parallel to the optical axis, and the position sensitive detector measures the position of the beam projection on the retina. The license was transferred to Tracey Technologies, Texas, United States, and the iTrace instrument is now in mass production as one of the best clinical aberrometers (Fig. 33).

In 1999, Navarro and Moreno-Barriuso[190] published their results on laser ray tracing based on electromechanical scanning with disappointing conclusions—ray tracing does not suit live eye studies since it requires several seconds for one measurement. In the iTrace, the output power of the CW laser diode is about 1 mW and the duration of projection in one point is 1 ms or less. Acousto-optic deflector switches the beam position with the transient time <10 μs. An example of the displayed data is presented in Fig. 33.

8 Ghost Laser Radars

Ghost imaging lidar is a modality requiring the comparison of the information from two channels (like imaging with

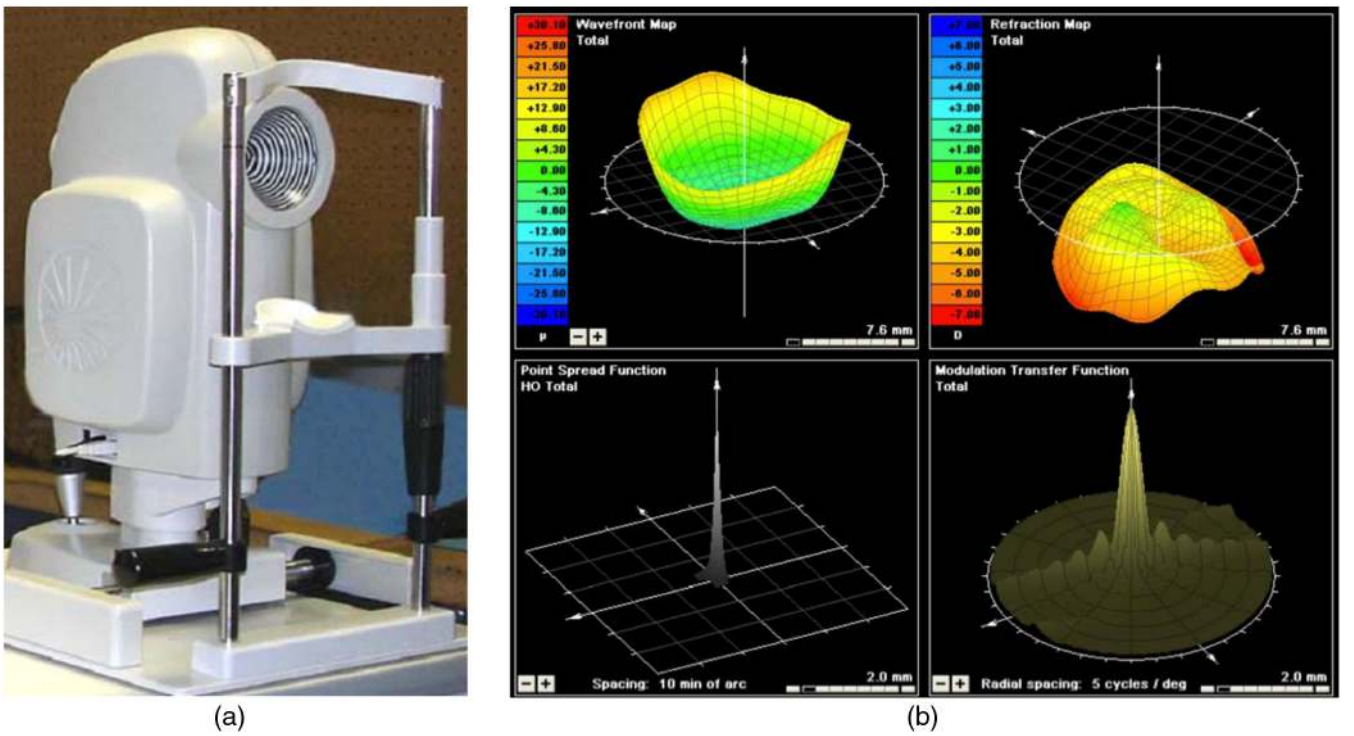

Fig. 33 (a) iTrace ray tracing aberrometer and (b) the displayed data.

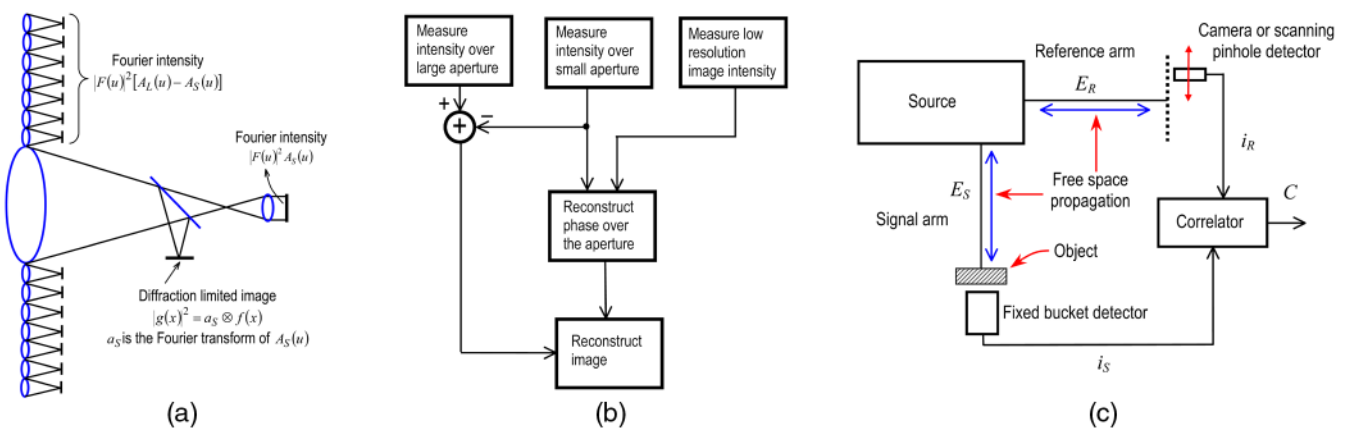

Fig. 34 (a) Principle of phase retrieval using a low-resolution image, (b) reconstruction of a fine-resolution image from the intensity measurements, and (c) ghost-imaging architecture.

coherent illumination, such as holography or OCT). The idea is to reconstruct a fine-resolution image using phase retrieval. It was described in 1990.[191] An array of point-size detectors samples the intensity of the optical field in the large aperture plane [Fig. 34(a)]. A beam splitter after the small-aperture telescope allows for the simultaneous detection of intensity in two planes: the usual focal plane, where there exists a diffraction-limited image of the object, and a Fourier transform of its small-aperture plane. Figure 34(b) is a block diagram depicting how these three intensity measurements are used to retrieve the phase over the large aperture and reconstruct a fine-resolution image.

The term "ghost imaging," which was coined soon after the initial experiments, emphasizes the fact that neither channel alone is sufficient to derive the target image. Only by correlating the two photocurrents you do have enough signal to make an image. Due to an intensive search by theoreticians for the best solution, the ghost imaging was called "a theme with variations".[192]

Many ghost-imaging experiments have been reported, both for transmission[193–196] and stand-off reflection.[197–199] Experiments suggest two correlated optical beams traversing distinct paths and impinging on two spatially separated photodetectors: one beam interacts with the target and then illuminates a single-pixel detector that provides no spatial resolution (reference channel), whereas the other beam traverses an independent path and impinges on a scanning pinhole detector or a high-resolution camera (signal channel) without any interaction with the target. The image is obtained by correlating the output photocurrents from these photodetectors [Fig. 34(c), shows an example of architecture for the case of image transmission].

Subsequent theoretical work addressed the impact of atmospheric turbulence[200] and turbulence combined with laser speckle[201] on ghost-imaging performance. These studies, and related experimental work,[177] delineated the conditions under which ghost imaging's spatial resolution becomes limited by turbulence, rather than diffraction.

A conventional laser radar that flood-illuminates a field of view has its spatial resolution's turbulence limit set by the atmospheric coherence length in the receiver's entrance pupil. On the other hand, a ghost imager, for the same environment, has its spatial resolution's turbulence limit set by the atmospheric coherence length in its structured-illuminator's exit pupil.[178] Therefore, for a bistatic configuration, when the atmospheric coherence length in the transmitter's exit pupil is significantly larger than the one in the receiver's entrance pupil, a ghost imager would yield better turbulence-limited spatial resolution than the conventional laser radar.

9 Conclusion

Laser radars have passed through many developmental stages since the first attempts to use lasers for ranging, which resulted in broad military applications for range finding and weapon guidance, especially laser designation, a form of bistatic laser radar. Further studies led to the development of laser imaging systems based on 2-D gated viewing, and then 3-D imaging, which is in the process of being fielded. Imaging systems are under intensive development including higher range and cross range resolution, single-photon sensitive arrays, multispectral or broad spectral emitting lasers for a variety of new capabilities like better weather penetration, capabilities to look through vegetation, through dense media, for target recognition, and other applications.

On the civilian and dual use side, we find that environmental laser radars are well established in remote sensing research of the atmosphere and the ocean while 3-D mapping laser radars have reached operational status, with 3-D mapping of large areas in many countries. Lasers are increasingly efficient and getting smaller and cheaper, for potential use in cars or unmanned vehicles. The use of lasers in self-driving cars is likely to be the first widespread commercial application of laser radar. This will significantly decrease the size, weight, and cost of laser radars. It also will enable widespread use of laser radars in UAVs as they proliferate for multiple commercial and military applications.

Laser radar technology is finding many applications in medicine. One of the examples is the optical low-coherence tomography originated from the lidar interferential reflectometry with its widespread use in ophthalmology for eye investigation with 3-D reconstruction of its structures, for 3-D endoscopic studies of blood vessels, amplified with Doppler 3-D velocimetry. Another great example is the refraction mapping of the human eye called aberrometry.

Emerging technologies and methods to be explored in laser radar systems include multiaperture and synthetic apertures, bistatic operation, multiwavelength or broad spectral emitting lasers, photon counting, and advanced quantum techniques as well as combined passive and active systems, and combining microwave and laser radars. We expect the use of coherent laser radar to increase as people find additional methods to utilize full field data, including phase information. On the component side, we foresee efficient versatile laser sources, compact solid state laser scanners for nonmechanical beam steering and beam forming, sensitive and larger focal plane arrays for both direct and coherent detection to be combined with efficient hardware and algorithms for processing of laser radar information and high data rates.

Comparison of achievements in laser radar technologies developed over the last 50 years across the globe shows the pervasive attraction of the laser radar technology and its applications.

References

1. G. W. Kamerman, "3D imaging laser radar," Lecture Course SC1103, *SPIE 2016 Defense+Security Symp. Technical Program*, p. 27, http://www.spie.org/conferences-and-exhibitions/defense--commercial-sensing/defense--security.
2. V. V. Molebny, *Optical Radar Systems: Basics of Functional Layouts (in Russian)*, p. 183, Mashinostroenie, Moscow (1981).
3. M. S. Malashin, R. P. Kaminskiy, and Y. B. Borisov, *Basics of Laser Radar System Design (in Russian)*, p. 208, Vysshaya Shkola, Moscow (1983).
4. I. N. Matveev et al., *Laser Radar Technology (in Russian)*, p. 272, Mashinostroenie, Moscow (1984).
5. P. F. McManamon, *Field Guide for Lidar*, p. 168, SPIE Press, Bellingham, Washington (2015).
6. P. F. McManamon, *Laser Radar. Progress and Opportunities in Active Electro-Optical Sensing*, Com. Chair, Study under Contract HHM402-10-D-0036-DO#10, The National Academies Press, Washington, DC (2014).
7. V. V. Molebny, *Optical Radar, (in Russian)*, p. 183, Kiev University Press, Kiev (1981).
8. R. R. Reibel et al., "Ultrabroadband optical chirp linearization for precision length metrology applications," *Opt. Lett.* **34**, 3692–3694 (2009).
9. J. M. Vaughan et al., "Coherent laser radar in Europe," *Proc. IEEE* **84**(2), 205–226 (1996).
10. P. McManamon, G. Kamerman, and M. Huffaker, "A history of laser radar in the United States," *Proc. SPIE* **7684**, 76840T (2010).
11. V. Molebny, P. Zarubin, and G. Kamerman, "The dawn of optical radar: a story from another side of the globe," *Proc. SPIE* **7684**, 76840B (2010).
12. V Molebny, G. Kamerman, and O. Steinvall, "Laser radar: from early history to new trends," *Proc. SPIE* **7835**, 783502 (2010).
13. T. Kobayashi, "Overview of laser remote sensing technology for industrial applications," in *Industrial Applications of Laser Remote Sensing*, T. Fukuchi and T Shiina, Eds., pp. 3–15, Bentham Science Publication, Sharjah, United Arab Emirates (2011).
14. H. Hu and J. Qiu, "An overview of lidar study in China," *Rev. Laser Eng.* **3**(2), 85–88 (1995).
15. A. A. Lebedev, "Optics herald," *Rozhdestvensky Opt. Soc. Bull.* **145**, 11–15 (2014).
16. P. A. Forrester and K. F. Hulme, "Laser range finders," *Opt. Quantum Electron.* **13**, 259–293 (1981).
17. V. P. Ponomarenko and A. M. Filachev, *Infrared Techniques and Electro-Optics in Russia: A History 1946–2006*, SPIE, Bellingham (2007).
18. Encyclopedia, "Weapons and technologies in Russia. XXI century," in *Electro-Optical Systems and Laser Technologies*, Vol. **11**, p. 720, Oruzhie i Tekhnologii, Moscow (2005).
19. J.-P. Fouilloy and M. B. Sirieix, "History of infrared optronics in France," *Proc. SPIE* **2552**, 804–814 (1995).
20. H. Raidt and D. H. Höhn, "Instantaneous intensity distribution in a focused laser beam at 0.63 μm and 10.6 μm, propagating through the atmosphere," *Appl. Opt.* **14**, 2747–2749 (1975).
21. Y. L. Kokurin, V. V. Kurbasov, and V. F. Lobanov, "Laser ranging of the light retroreflector installed on the "Lunokhod-1" (in Russian), *Kvantovaya Elektronika* **5**, 138 (1971).
22. N. Sugimoto et al., "Earth-satellite-earth laser long-path absorption experiment using the Retroreflector in Space (RIS) on the Advanced Earth Observing Satellite (ADEOS)," *J. Opt. A: Pure Appl. Opt.* **1**, 201–209 (1999).
23. D. E. Smith et al., "Initial observations from the lunar orbiter laser altimeter (LOLA)," *Geophys. Res. Lett.* **37**, L18204 (2010).
24. D. Inoue et al., "Highly sensitive LIDAR with a thumb-sized sensor-head built using an optical fiber preamplifier," *Proc. SPIE* **8731**, 87310Y (2013).
25. S. Yamashita and T. Okoshi, "Performance improvement and optimization of fiber amplifier with a midway isolator," *IEEE Photonics Technol. Lett.* **4**(11), 1276–1278 (1992).
26. T. Hashimoto, T. Kubota, and T. Mizuno, "Light weight sensors for the autonomous asteroid landing of MUSES-C mission," *Acta Astronaut.* **52**, 381–388 (2003).

27. T. Mizuno et al., "Evaluation of LIDAR system in rendezvous and touchdown sequence of Hayabusa mission," *Trans. Jpn. Soc. Aeronaut. Space Sci.* **53**, 47–53 (2010).
28. M. J. Taylor et al., "Pulsed CO_2 TEA laser rangefinder," *Appl. Opt.* **17**, 885–889 (1978).
29. H. Karning, J. F. Ruger, and M. Weispfenning, "Concept and design of a multiple-function laser (MFL)," *Proc. SPIE* **3436**, 433–438 (1998).
30. T. Wilkerson et al., "VisibleWindTM: a rapid-response system for high-resolution wind profiling," *Proc. SPIE* **7460**, 746009 (2009).
31. Z. Liu et al., "Low-altitude atmospheric wind measurement from the combined Mie and Rayleigh backscattering by Doppler lidar with an iodine filter," *Appl. Opt.* **41**, 7079–7086 (2002).
32. X. Dou et al., "Mobile Rayleigh Doppler lidar for wind and temperature measurements in the stratosphere and lower mesosphere," *Opt. Express* **22**, A1203–A1221 (2014).
33. H. Xia et al., "Stratospheric temperature measurement with scanning Fabry–Perot interferometer for wind retrieval from mobile Rayleigh Doppler lidar," *Opt. Express* **22**, 21776–21789 (2014).
34. C. L. Korb et al. "Theory of the double-edge technique for Doppler lidar wind measurement," *Appl. Opt.* **37**, 3097–3104 (1998).
35. N. Martin, R. Ganini, and X. Chazelle, "CLARA-A Franco-British development of airborne laser radar," in *Proc. 7th Conf. on Coherent Laser Radar, Applications & Technology*, Paris (1993).
36. B. Stephan and P. Metivier, "Flight evaluation trials of a heterodyne CO_2 laser radar," *Proc. SPIE* **0806**, 9 (1987).
37. R. D. Callan et al., "Active airborne line scan experiment," *Proc. SPIE* **2272**, 183–191 (1994).
38. D. Pierrottet et al., "Flight test performance of a high precision navigation Doppler lidar," *Proc. SPIE* **7323**, 732311 (2009).
39. S. W. Henderson et al., "Wind Lidar," in *Laser Remote Sensing*, T. Fujii and T. Fukuchi, Eds., pp. 469–722, CRC Taylor & Francis, Boca Raton, Florida (2005).
40. J. M. Vaughan et al., "Coherent laser radar in Europe," *Proc. IEEE* **84**(2), 205–226 (1996).
41. D. K. Killinger and A. Mooradian, Eds., *Optical and Laser Radar Remote Sensing*, pp. 318–381, Springer, Berlin, Heidelberg (1983).
42. R. M. Huffaker, A. V. Jelalian, and J. A. L. Thompson, "Laser-Doppler system for detection of aircraft trailing vortices," *Proc. IEEE* **58**, 322–326 (1970).
43. T. Sakimura et al., "1.5-μm high-gain and high-power laser amplifier using a Er, Yb:glass planar waveguide for coherent Doppler lidar," in *Proc. CLEO*, San Jose, p. 114 (2012).
44. S. Kameyama et al., "Development of wind sensing coherent Doppler lidar at Mitsubishi Electric Corporation from late 1990s to 2013," in *Abstracts Int. Coherent Laser Radar Conf.* (2013).
45. K. F. Hulme et al., "A CO_2 laser rangefinder using heterodyne detection and chirp pulse compression," *Opt. Quantum Electron.* **13**, 35–45 (1981).
46. J. L. Meyzonette, B. Remy, and G. Saccomani, "A coherent laser radar with chirp compression," *Proc. SPIE* **783**, 169–179 (1987).
47. P. H. Davies et al., "An FM-CW laser radar with electro-optic intracavity modulation," *Proc SPIE* **1181**, 285–290 (1989).
48. G. Sepp, "Moving target detection with compact laser Doppler radar," *Proc. SPIE* **1181**, 296–300 (1989).
49. I. Renhorn, B. Broberg, and K. Vilhelmsson, "Coherent laser radar based on semiconductor technology," in *Proc. CLEO*, Europe, Amsterdam (1994).
50. C. J. Karlsson et al., "All-fiber multifunction continuous-wave coherent laser radar at 1.55 μm for range, speed, vibration, and wind measurements," *Appl. Opt.* **39**, 3716–3726 (2000).
51. P. Lutzmann et al., "Laser vibration sensing: overview and applications," *Proc. SPIE* **8186**, 818602 (2011).
52. K. I. Schultz and S. Fisher, "Ground-based laser radar measurements of satellite vibrations," *Appl. Opt.* **31**, 7690–7695 (1992).
53. K. I. Schultz et al., "Satellite vibration measurements with an autodyne CO_2 laser radar," *Appl. Opt.* **33**, 2349–2355 (1994).
54. A. L. Kachelmyer and K. I. Schultz, "Laser vibration sensing," *Lincoln Lab. J.* **8**(1), 3–28 (1995).
55. F. Hanson and M. Lasher, "Coherent laser radar at 3.6 μm," *Appl. Opt.* **41**, 7689–7693 (2002).
56. G. M. Revel et al., "Laser vibrometry vibration measurements on vehicle cabins in running conditions: helicopter mock-up application," *Opt. Eng.* **50**, 101502 (2011).
57. J. C. van den Heuvel et al., "Laser-induced acoustic landmine detection with experimental results on buried landmines," *Proc. SPIE* **5415**, 51–60 (2004).
58. G. Fiocco and L. O. Smullin, "Detection of scattering layers in the upper atmosphere (60–140 km) by optical radar," *Nature* **199**, 1275–1276 (1963).
59. R. T. H. Collis, F. G. Fernald, and M. G. H. Ligda, "Laser radar echoes from the clear atmosphere," *Nature* **203**, 508–508 (1964).
60. R. M. Schotland, "The determination of the vertical profile of atmospheric gases by means of a ground based optical radar," in *Proc. Third Symp. on Remote Sensing of Environment (1964)*, U. Michigan (1965).
61. H. Inaba et al., "Fundamental study of operational performance of a laser radar system employing A-scope representation," *Electron. Commun. Jpn.* **51-B**, 36–52 (1968).
62. Y. F. Arshinov, S. M. Bobrovnikov, and S. V. Sapozhnikov, "On the technique of lidar measurement of the atmosphere temperature by signals ratio of the pure rotational spectra of N_2 and O_2," *Zhurnal Prikladnoy Spektroskopii* **32**(4), 725–731 (1980) (in Russian).
63. V. E. Zuev, Y. S. Makushkin, and V. N. Matrichev, "Laser sensing of the humidity profile of the atmosphere," *Doklady AN SSSR* **257**(6), 1338–1342 (1981) (in Russian).
64. S. Ivanov, Ed., *Weapons and Technologies in Russia. XXI Century*, p. 720, Oruzhie i Tekhnologii, Moscow (2005).
65. ASDM-Lidar, http://www.npk-spp.ru/deyatelnost/ekomonitoring.html (5 December 2016).
66. H. Hu and J. Qiu, "An overview of lidar study in China," *Rev. Laser Eng.* **23**(2), 85–88 (1994).
67. S. Svanberg, *Atomic and Molecular Spectroscopy: Basic Aspects and Applications*, Springer, Berlin (2004).
68. E. D. Hinkley, Ed., *Laser Monitoring of the Atmosphere*, Springer, Berlin (1976).
69. T. Fujii and T. Fukuchi, *Laser Remote Sensing*, CRC Press, Boca Raton, Florida (2005).
70. A. P. Ivanov, *Optics of Scattering Media (in Russian)*, p. 592, Nauka i Tekhnika, Minsk (1969).
71. A. P. Ivanov, *Physical Fundamentals of Hydro-Optics (in Russian)*, p. 504, Nauka i Tekhnika, Minsk (1975).
72. V. I. Tatarskiy, *Wave Propagation in Turbulent Atmosphere (in Russian)*, p. 548, Nauka, Moscow (1967).
73. V. E. Zuev, *Propagation of Laser Radiation in Atmosphere (in Russian)*, p. 287, Radio i Sviaz, Moscow (1981).
74. A. S. Gurvich et al., *Laser Radiation in the Turbulent Atmosphere (in Russian)*, p. 277, Nauka, Novosibirsk (1976).
75. V. A. Banakh and V. L. Mironov, *Propagation of Laser Radar Radiation in the Turbulent Atmosphere (in Russian)*, p. 174, Nauka, Novosibirsk (1986).
76. V. M. Zakharov and O. K. Kostko, *Meteorological Laser Radars (in Russian)*, p. 221, Hydrometeoizdat, Leningrad (1977).
77. R. R. Agishev, *Lidar Monitoring of the Atmosphere (in Russian)*, p. 314, Fizmatgiz, Moscow (2009).
78. A. M. Wyant and C. R. Philbrick, "Atmospheric aerosol characterization using multiwavelength multistatic light scattering," *Proc. SPIE* **7684**, 76840I (2010).
79. C. R. Philbrick et al., "Optical remote sensing techniques to characterize the properties of atmospheric aerosols," *Proc. SPIE* **7684**, 76840J (2010).
80. Q. He and J. Mao, "Observation of urban mixed layer at Beijing using a micro pulse lidar (in Chinese)," *Acta Meteorol. Sinica* **63**, 374–384 (2005).
81. Q. He et al., "A study of evolution and dynamics of urban atmospheric mixing-layer depth based on lidar data and numerical simulation," *Chin. J. Atmos. Sci.* **30**, 293 (2006).
82. Q. S. He et al., "Observational and modeling studies of urban atmospheric boundary-layer height and its evolution mechanisms," *Atmos. Environ.* **40**, 1064–1077 (2006).
83. S. Yuan, X. Yu, and J. Zhou, "Lidar observations of the lower atmospheric layer in Hefei (in Chinese)," *Chin. J. Atmos. Sci.* **29**, 387–395 (2005).
84. J. Zhou et al., "Vertical distribution and temporal variation of Asian dust observed by lidar over Hefei, China," *J. Korean Phys. Soc.* **49**, 320–326 (2006).
85. T. Murayama et al., "Ground-based network observation of Asian dust events of April 1998 in east Asia," *J. Geophys. Res.* **106**, 18345–18359 (2001).
86. J. Zhou et al., "LIDAR observation of Asian dust over Hefei, China, in spring 2000," *J. Geophys. Res.* **107**, 4252–4259 (2002).
87. D. Wu et al., "12-year LIDAR observations of tropospheric aerosol over Hefei (31.9°N, 117.2°E), China," *J. Opt. Soc. Korea* **15**(1), 90–95 (2011).
88. J. Zhou, H. Hu, and Z. Gong, "Lidar obserbations of Mt. Pinatubo cloud over Hefei," *Chin. Sci. Bul.* **38**(16), 1373–1376 (1993).
89. J. Qiu et al., *Paper Abstract of 17th International Laser Radar Conference (ILRC)*, Sendai, Japan, pp. 119–122 (1994).
90. H. Hu, "Lidar activity in China," in *Paper Abstract of 17th ILRC*, Sendai, Japan (1994).
91. S. Hu et al., "Differential absorption lidar for environmental SO_2 measurements (in Chinese)," *Chin. J. Laser* **31**, 1121–1126 (2004).
92. S. Hu et al., "A new differential absorption lidar for NO_2 measurements using Raman-shifted technique," *Chin. Opt. Lett.* **1**, 435–437 (2003).
93. Y. Wang et al., "Observation and analysis of the temperature inversion layer by Raman lidar up to the lower stratosphere," *Appl. Opt.* **54**, 10079–10088 (2015).
94. C. Xie et al., "New mobile Raman lidar for measurement of tropospheric water vapor (in Chinese)," *Acta Opt. Sin.* **26**, 1281–1286 (2006).
95. J. Mao et al., "Accurate temperature profiling of the atmospheric boundary layer using an ultraviolet rotational Raman lidar," *Opt. Commun.* **282**(15), 3113–3118 (2009).

96. Y. Wang et al., "Observations of atmospheric water vapor, aerosol, and cloud with a Raman lidar," *Opt. Eng.* **53**(11), 114105 (2014).
97. Y. Wang et al., "Observation and analysis of the temperature inversion layer by Raman lidar up to the lower stratosphere," *App. Opt.* **54**, 10079–10088 (2015).
98. S. Gong et al., "First time observation of sodium layer over Wuhan, China by sodium fluorescence lidar," *Sci. China A* **40**(11), 1228–1232 (1997).
99. S. Gong et al., "Lidar activity at Wuhan Institute of Physics and Mathematics, China," *Proc. SPIE* **4893**, 8 (2003).
100. X. Dou et al., "A statistical study of sporadic sodium layer observed by sodium lidar at Hefei (31.8°N, 117.3°E)," *Ann. Geophys.* **27**, 2247–2257 (2009).
101. F. Yi et al., "Lidar observations of sporadic Na layers over Wuhan (30.5°N, 114.4°E)," *Geophys. Res. Lett.* **29**, 59-1–59-4 (2002).
102. F. Yi et al., "Simultaneous observations of sporadic Fe and Na layers by two closely collocated resonance fluorescence lidars at Wuhan (30.5°N, 114.4°E), China," *J. Geophys. Res.* **112**, D04303 (2007).
103. X. Hu et al., "Sodium fluorescence Doppler lidar to measure atmospheric temperature in the mesopause region," *Chin. Sci. Bull.* **56**, 4–13 (2011).
104. H. Inaba and T. Kobayashi, "Laser-Raman radar for chemical analysis of polluted air," *Nature* **224**, 170–172 (1969).
105. S. Nakahara et al., "Mobile laser Raman radar for monitoring stack plume," *IEEE J. Quantum Electron.* **7**, 325–325 (1971).
106. M. R. Bowman, A. J. Gibson, and M. C. W. Sandford, "Atmospheric sodium measured by a tuned laser radar," *Nature* **221**, 456–457 (1969).
107. T. Aruga et al., "Laser radar observation of the sodium layer in the upper atmosphere," *Report Ionos. Space Res. Jpn.* **28**, 65–68 (1974).
108. C. Nagasawa, M. Hirono, and M. Fujiwara, "A reliable efficient forced oscillator dye laser to measure the upper atmospheric sodium layer," *Jpn. J. Appl. Phys.* **19**(1), 143–147 (1980).
109. O. Uchino et al., "Measurement of stratospheric vertical ozone distribution with a XeCl lidar: estimated influence of aerosols," *Appl. Opt.* **19**, 4175 (1980).
110. O. Uchino et al., "Differential-absorption-lidar measurement of tropospheric ozone with excimer-Raman hybrid laser," *Opt. Lett.* **8**, 347–349 (1983).
111. M. Nakazato et al., "Tropospheric ozone differential-absorption lidar using stimulated Raman scattering in carbon dioxide," *Appl. Opt.* **46**, 2269–2279 (2007).
112. T. Shibata, M. Kobuchi, and M. Maeda, "Measurements of density and temperature profiles in the middle atmosphere with a XeF lidar," *Appl. Opt.* **25**, 685–688 (1986).
113. H. Shimizu et al., "Large scale laser radar for measuring aerosol distribution over a wide area," *Appl. Opt.* **24**, 617–647 (1985).
114. Y. Sasano, H. Shimizu, and N. Takeuchi, "Convective cell structures revealed by Mie laser radar observations and image data processing," *Appl. Opt.* **21**, 3166–3169 (1982).
115. H. Nakane and Y. Sasano, "Structure of a sea-breeze front revealed by scanning lidar observation," *J. Meteorol. Soc. Jpn.* **64**, 787–792 (1986).
116. A. B. Geschwendtner and W. E. Keicher, "Development of coherent laser radar at Lincoln Laboratory," *Lincoln Lab. J.* **12**(2), 383–396 (2000).
117. J. G. Verly and R. L. Delanoy, "Model-based automatic target recognition (ATR) system for forward looking ground-based and airborne imaging laser radars (LASER RADAR)," *Proc. IEEE* **84**(2), 126–163 (1996).
118. A. V. Jelalian, *Laser Radar Systems*, Artech House, Boston (1992).
119. G. R. Osche and D. S. Young, "Imaging laser radar in the near and far infrared," *Proc. IEEE* **84**(2), 103–125 (1996).
120. C. C. Andressen, "A 1.32 μm long range solid state imaging laser radar," *Proc. SPIE* **1694**, 121–130 (1992).
121. G. Stevenson et al., "Testing the helicopter obstacle avoidance system," *Proc. SPIE* **2472**, 93–103 (1995).
122. J. L. Meyzonnette, B. Remy, and G. Saccomani, "Imaging CO_2 laser radar with chirp pulse compression," *Proc SPIE* **783**, 169–179 (1987).
123. C. J. Karlsson et al., "All-fiber multifunction continuous-wave coherent laser radar at 1.55 μm for range, speed, vibration, and wind measurements," *Appl. Opt.* **39**, 3716–3726 (2000).
124. H. Ahlberg et al., "Imaging Q-switched CO_2 laser radar with heterodyne detection: design and evaluation," *Appl. Opt.* **25**, 2891–2898 (1986).
125. D. Letalick, I. Renhom, and O. Steinvall, "Measured signal amplitude distributions for a coherent FM-cw CO_2 laser radar," *Appl. Opt.* **25**, 3927–3938 (1986).
126. D. Letalick, M. Millnert, and I. Renhorn, "Terrain segmentation using laser radar range data," *Appl. Opt.* **31**, 2883–2890 (1992).
127. A. F. Milton, G. Klager, and T. Bowman, "Low cost sensors for UGVs," *Proc. SPIE* **4024**, 180–191 (2000).
128. R. L. Espinola et al., "Modeling the target acquisition performance of active imaging systems," *Opt. Express* **15**, 3816–3832 (2007).
129. T. Chevalier and O. Steinvall, "Laser radar modelling for simulation and performance evaluation," *Proc. SPIE* **7482**, 748206 (2009).
130. P. Andersson, "Long range 3D imaging using range gated laser radar images," *Opt. Eng.* **45**(3), 034301 (2006).
131. O. Steinvall et al., "Overview of range gated imaging at FOI," *Proc. SPIE* **6542**, 654216 (2007).
132. E. Repasi et al., "Advanced short-wavelength infrared range- gated imaging for ground applications in monostatic and bistatic configurations," *Appl. Opt.* **48**, 5956–5969 (2009).
133. O. Steinvall et al., "Laser imaging of small surface vessels and people at sea," *Proc SPIE* **7684**, 768417 (2010).
134. D. Bonnier, S. Lelievre, and L. Demers, "On the safe use of long-range laser active imager in the near-infrared for homeland security," *Proc. SPIE* **6206**, 620601 (2006).
135. D. O. Schneider and R. Israeli, "Advance in active night vision for filling the gap in remote sensing," *Proc. SPIE* **7482**, 748203 (2009).
136. P. Heckman and R. T. Hodgson, "Underwater optical range gating," *IEEE J. Quantum Electron.* **3**, 445–448 (1967).
137. G. R. Fournier et al., "Range-gated underwater laser imaging system," *Opt. Eng.* **32**, 2185–2190 (1993).
138. M. P. Strand, "Underwater electro-optical system for mine identification," *Proc. SPIE* **2496**, 487–497 (1995).
139. J. Busck and H. Heiselberg, "High accuracy 3D laser radar," *Proc. SPIE* **5412**, 257–264 (2004).
140. H. M. Tulldahl and M. Pettersson, "Lidar for shallow underwater target detection," *Proc. SPIE* **6739**, 673906 (2007).
141. S. Bailey et al., "Advances in HgCdTe APDs and LASER RADAR receivers," *Proc. SPIE* **7660**, 766031 (2010).
142. E. de Borniol et al., "HgCdTe-based APD focal plane array for 2D and 3D active imaging: first results on a 320 × 256 with 30 μm pitch demonstrator," *Proc. SPIE* **7660**, 76603D (2010).
143. A. Ashcroft and I. Baker, "Developments in HgCdTe avalanche photodiode technology and applications," *Proc. SPIE* **7660**, 76603C (2010).
144. R. Heinrichs et al., "Three-dimensional laser radar with APD arrays," *Proc. SPIE* **4377**, 106–117 (2001).
145. J. P. Donnelly et al., "1-μm Geiger-mode detector development," *Proc. SPIE* **5791**, 281–287 (2005).
146. R. M. Marino and W. R. Davis, "Jigsaw: a foliage-penetrating 3D imaging laser radar system," *Lincoln Lab. J.* **15**, 23–36 (2005).
147. P. Cho et al., "Real-time 3D laser radar imaging," *Lincoln Lab. J.* **16**(1) 147–164 (2006).
148. A. Kolb and R. Koch, "Dynamic 3D imaging," in *Proc. of the DAGM Workshop in Jena*, 177 p., Springer, Berlin-Heidelberg (2009)
149. C. Grönwall et al., "An approach to target detection in forested scenes," *Proc. SPIE* **6950**, 69500S (2008).
150. W. Armbruster, "Exploiting range imagery: techniques and applications," *Proc. SPIE* **7382**, 738203 (2009).
151. http://www.darpa.mil/ipto/programs/spi3d/spi3d.asp.
152. http://www.fas.org/man/dod-101/sys/smart/docs/locaas_Industry_Day/sld013.htm.
153. http://www.afcea.org/signal/articles/anmviewer.asp?a=1099&print=yes.
154. C. Andressen et al., "Tower test results for an imaging LASER RADAR seeker," *Proc. SPIE* **5791**, 70–82 (2005).
155. C. Seidel, I. Schwartz, and P. Kielhorn, "Helicopter collision avoidance and brown-out recovery with HELLAS," *Proc. SPIE* **7114**, 71140G (2008).
156. R. Stettner and H. Bailey, "Eye-safe laser radar 3D imaging," *Proc. SPIE* **4377**, 46–56 (2001).
157. M. A. Albota et al., "Three-dimensional imaging laser radar with a photon-counting avalanche photodiode array and microchip laser," *Appl. Opt.* **41**, 7671 (2002).
158. S. Kameyema et al., "Development of long range, real-time, and high resolution 3D imaging laser radar," *Proc. SPIE* **8192**, 819205 (2011).
159. H. Tsuji et al., "Pulsed 3D laser sensor with scan-less receiver," *Proc. SPIE* **8379**, 837904 (2012).
160. C. M. Wong et al., "Automated in-track and cross-track airborne flash LASER RADAR image registration for wide-area mapping," *Proc. SPIE* **7684**, 76840S (2010).
161. E. G. P. Bovenkamp and K. Schutte, "Laser gated viewing: an enabler for automatic target recognition," *Proc. SPIE* **7684**, 76840Z (2010).
162. T. S. Lewis and H. S. Hutchins, "A synthetic aperture at 10.6 microns," *Proc. IEEE* **58**, 1781–1782 (1970).
163. C. C. Aleksof et al., "Synthetic aperture imaging with a pulsed CO_2 TEA laser," *Proc. SPIE* **783**, 29–41 (1987).
164. S. Marcus, B. O. Colella, and T. J. Green, "Solid-state laser synthetic aperture radar," *Appl. Opt.* **33**, 960–964 (1994).
165. T. J. Green, S. Marcus, and B. O. Colella, "Synthetic-aperture-radar imaging with a solid-state laser," *Appl. Opt.* **34**, 6941–6949 (1995).
166. P. Park and J. H. Shapiro, "Performance analysis of optical synthetic aperture radars," *Proc. SPIE* **999**, 100–116 (1988).
167. S. Yoshikado and T. Aruga, "Feasibility study of synthetic aperture infrared laser radar techniques for imaging of static and moving objects," *Appl. Opt.* **37**, 5631–5639 (1998).
168. T. G. Kyle, "High resolution laser imaging system," *Appl. Opt.* **28**, 2651–2656 (1989).
169. J. Shan and C. K. Toth, *Topograhic Laser Ranging and Scanning—Principles and Processing*, CRC Press, Boca Raton, Florida (2009).
170. "Leica AHAB DragonEye Dual Head. Oblique LiDAR System," 2014, http://www.airbornehydro.com/sites/default/files/Leica%20AHAB%20DragonEye%20DH.pdf (1 October 2016).

171. K. P. Corbley, "Geiger-mode L iDAR delivers fast, wide-area mapping," 2015, http://eijournal.com/print/articles/geiger-mode-lidar-delivers-fast-wide-area-mapping (1 October 2016).
172. "Optech Lynx SG mobile mapper," http://www.teledyneoptech.com/index.php/product/lynx-sg1 (1 October 2016).
173. "All the distance sensing data you will ever need," http://velodynelidar.com/products.html (1 October 2016).
174. J. Banic and G. Cunningham, "Airborne laser bathymetry: a tool for the next millennium," 2006, http://www.jalbtcx.org/downloads/publications/32banic_cunningham_98.pdf (1 October 2016).
175. W. J. Lillycrop, L. E. Parson, and J. L. Irish, "Development and operation of the SHOALS airborne lidar hydrographic survey system," *Proc. SPIE* **2964**, 26–37 (1996).
176. A. G. Cunningham et al., "Shallow water laser bathymetry: accomplishments and applications," in *Proc. Oceanology Int.*, Vol. 3, pp. 277–288 (1998).
177. G. C. Guenther et al., "Meeting the accuracy in airborne lidar bathymetry," in *Proc. EARSeL-SIG-Workshop LIDAR*, Dresden/FRG, June 16–17 (2000).
178. R. Nairn, "Royal Australian Navy laser airborne depth sounder, the first year of operations," *Int. Hydro. Rev. Monaco* **71**(1), 109–119 (1994).
179. W. J. Lillycrop, J. L. Irish, and L. E. Parson, "SHOALS system: three years of operation with airborne lidar bathymetry—experiences, capability and technology advancements," *Sea Technol.* **38**(6), 17–26 (1997).
180. O. Steinvall and K. Koppari, *Lidar Depth Sounding—An Overview of Swedish Activities and With Future Prospects*, pp. 2–25, SPIE, Bellingham (1996).
181. T. Dresel, G. Häusler, and H. Venzke, "Three-dimensional sensing of rough surfaces by coherence radar," *Appl. Opt.* **31**, 919–925 (1992).
182. B. E. Bouma and G. J. Tearney, Eds., *Handbook of Optical Coherence Tomography*, p. 509, Marcel Dekker, Inc., Basel (2002).
183. F. Drexler and J. G. Fujimoto, *Optical Coherence Tomography. Technology and Applications*, 2nd ed., p. 2571, Springer, Switzerland (2015).
184. A. Girach and R. C. Sergott, *Optical Coherence Tomography*, p. 148, Springer, Switzerland (2016).
185. V. J. Srinivasan et al., "OCT methods for capillary velocimetry," *Biomed. Opt. Express* **3**(3), 612–629 (2012).
186. H. M. Varma et al., "Speckle contrast optical tomography: a new method for deep tissue three-dimensional tomography of blood flow," *Biomed. Opt. Express.* **5**, 1275–1289 (2014).
187. V. V. Molebny et al., "Retina ray-tracing technique for eye-refraction mapping," *Proc. SPIE* **2971**, 175–183 (1997).
188. V. V. Molebny et al., "High precision double-frequency interferometric measurement of the cornea shape," *Proc. SPIE* **2965**, 121–126 (1996).
189. V. V. Molebny et al., "Adaptive optics technique for measuring eye refraction distribution," *Proc. SPIE* **2930**, 147–156 (1996).
190. R. Navarro and E. Moreno-Barriuso, "Laser ray-tracing method for optical testing," *Opt. Lett.* **24**, 951–953 (1999).
191. J. R. Fienup and A. M. Kowalczyk, "Phase retrieval for a complex-valued object by using a low-resolution image," *J. Opt. Soc. Am. A.* **7**(3), 450–458 (1990).
192. J. H. Shapiro, "Ghost imaging: a theme with variations," in *Proc. Imaging and Applications Optics*, OSA (2015).
193. F. Ferri et al., "High-resolution ghost image and ghost diffraction experiments with thermal light," *Phys. Rev. Lett.* **94**, 183602 (2005).
194. G. Scarcelli, V. Berardi, and Y. Shih, "Can two-photon correlation of chaotic light be considered as correlation of intensity fluctuations?," *Phys. Rev. Lett.* **96**, 063602 (2006).
195. F. Ferri et al., "Differential ghost imaging," *Phys. Rev. Lett.* **104**, 253603 (2010).
196. J. H. Shapiro and R. W. Boyd, "The physics of ghost imaging," *Quantum Inf. Process.* **11**, 949–993 (2012).
197. R. Meyers, K. S. Deacon, and Y. Shih, "Ghost-imaging experiment by measuring reflected photons," *Phys. Rev. A* **77**, 041801 (2008).
198. P. B. Dixon et al., "Quantum ghost imaging through turbulence," *Phys. Rev. A* **83**, 051803 (2011).
199. B. I. Erkmen, "Computational ghost imaging for remote sensing," *J. Opt. Soc. Am. A.* **29**(5), 782–789 (2012).
200. J. Cheng, "Ghost imaging through turbulent atmosphere," *Opt. Express* **17**, 7916–7921 (2009).
201. N. D. Hardy and J. H. Shapiro, "Reflective ghost imaging through turbulence," *Phys. Rev.* **A84**, 063824 (2011).

Vasyl Molebny received his PhD in1965, and his DSc degree in optical radars in 1991. He is a professor of optics at the National University of Kyiv. He is an inventor of ray tracing aberrometry. His interests are precision laser radar systems and wavefront measurements. He has more than 300 publications. He is a member of Academy of Technological Sciences and of Optical Society, Ukraine. He received national prize of Russia and Academician Glushkov award. Until 2001, he was the VP of Kvant Scientific Research Institute and designer-in-chief of laser-based systems.

Paul McManamon is a president of Exciting Technology and Technical Director LOCI, University of Dayton. He has chaired laser radar study for the National Academy of Sciences and cochaired "Optics and Photonics, Essential Technologies for Our Nation." He is a fellow of SPIE, IEEE, OSA, AFRL, DEPs, MSS, and AIAA. He is the president of SPIE in 2006. Until May 2008, he was a chief scientist, AFRL sensors directorate, and responsible for AFRL sensing technologies, recognition, CM, and warfare technologies. He received the Meritorious Presidential Rank Award in 2006.

Ove Steinvall received his MS degree from Uppsala in 1969 and his PhD from Chalmers Institute of Technology in 1974. He has been employed by the National Defense Research Establishment (FOI) since 1969. He is a research director in laser systems. He is an associate professor at Chalmers Institute of Technology. His activities involve laser CM, laser radars, and free-space laser communications. He has 110 papers and 300 reports. He is a fellow of SPIE, senior member of OSA, Swedish Optical Society, and the Royal Academic of Military Sciences. He received three national and NATO awards. He is a chair of numerous laser conferences.

Takao Kobayashi graduated from Tohoku University, Sendai, in 1966. He received his DEng degree from Tohoku University in 1977. He is a research associate at Tohoku, since 1967. Since 1981, he is a professor of University of Fukui. He is an honorary professor in 2007. He is a visiting researcher at Yale University, USA, from 1978 to 1979. His research involves laser remote sensing (lidar) and solid-state laser and photonics. He served as a member of numerous scientific, evaluation, and program committees in laser sensing. He is serving as a chair of the Laser Radar Society of Japan (LRSJ) and a visiting researcher of RIKEN.

Weibiao Chen received his PhD from Ocean University of China in 1997. He joined Shanghai Institute of Optics and Fine Mechanics in 2000. He worked in laser remote sensing for atmosphere and oceanography and laser communication. He is a director of Laboratory of Space Laser Communication and Lidar in 2008 and a vice-director of SIOM in 2009. His team developed airborne laser bathymetry, the first spaceborne Chinese Lunar explorer, and working on spaceborne atmospheric lidar. He is a fellow of Chinese Optical Society. He is the author and coauthor of ~70 scientific papers.